Quantum control of two critically dressed spin-1/2 species in magnetic fluctuations

Raymond Tat and C. M. Swank
Division of Physics, Math and Astronomy, California Institute of Technology, Pasadena, California 91125, USA

(Received 3 December 2021; revised 14 April 2022; accepted 11 May 2022; published 25 May 2022)

The neutron electric dipole moment experiment at the Spallation Neutron Source (nEDM@SNS experiment) proposes to measure the nEDM using the spin-dependent capture cross section of neutrons on ^{3}He. The critical dressing mode of this experiment uses an oscillating magnetic field to dress the gyromagnetic ratios of neutrons and ^{3}He to the same value. While this technique grants increased sensitivity to the nEDM by improving the signal-to-noise ratio, this mode of measurement also introduces additional noise from the power supply used to drive the dressing field. This can lead to randomly fluctuating magnetic fields which cause the spins of neutrons and ^{3}He to drift apart over time. Here we use second-order time-dependent perturbation theory to compute relaxation and frequency shifts due to fluctuations in the dressing field in terms of the magnetic field noise power spectrum and compare these calculations to numerical solutions obtained by integrating the Bloch equations. We then use these results to develop mitigation strategies for this type of noise. Furthermore, we report on spin dressing modulation techniques that significantly amplify coherence times for the critically dressed system, and attempt to quantify the achievable coherence time.

DOI: 10.1103/PhysRevA.105.053120

I. INTRODUCTION

When a particle's spin precessing in a static magnetic field is exposed to an off-resonant oscillating orthogonal magnetic field, the effective gyromagnetic ratio of the particle—and thus its precession frequency—is modified. This phenomenon is known as spin dressing and was first studied theoretically in Ref. [1]. Spin dressing is found to have applications across multiple subfields in quantum information and fundamental physics, including increasing coherence time of free induction decay (FID) in relatively large magnetic field gradients [2,3]. The use of multiple dressing frequencies tuned to extend the coherence of atomic clocks in field gradients was first reported in Ref. [4], whereas the authors of Ref. [5] used this technique to mitigate Stark shifts. With multiple dressing field directions, enhanced spin manipulation for quantum information is achievable and can even accelerate the effective Larmor precession; this is discussed in Refs. [6,7]. In Ref. [8], the authors found that critical spin dressing (CSD), the simultaneous dressing of two spin species to the same Larmor frequency, can be applied for a very sensitive measurement of the neutron electric dipole moment (nEDM). A detailed investigation in Ref. [9] found that this technique would halve the statistical uncertainty of an nEDM measurement compared to an analogous measurement using FID. Additionally, by modulating the parameters of CSD as described in Refs. [3,8], systematic uncertainty from phase fluctuations not associated with noise in the spin dressing field (e.g., external magnetic field drifts) is significantly reduced even without correction from a comagnetometer. For example, with modulation at the angular frequency ω_m, phase accumulation from slow field drifts in the apparatus will be modified by a factor $\sim 1/\sqrt{\omega_m}$ [10].

In the nEDM at the Spallation Neutron Source (nEDM@SNS) experiment, ultracold neutrons (UCNs) are confined to a pair of acrylic (polymethylmethacrylate, PMMA) measurement cells with dimensions $L_x \times L_y \times L_z = 40 \times 10.2 \times 7.6$ cm in solution with polarized ^{3}He in superfluid ^{4}He. A large electrode sits between the two cells, which are sandwiched by ground electrodes on either side and provide a large electric field of the order of 7.5 MV/m between each cell in the $\hat{z}$ direction so the electric field strength has opposite sign for each cell. A superconducting persistent $\cos\theta$ coil provides a static uniform magnetic field of magnitude $B_0 \geqslant 3\ \mu$T along the $\hat{z}$ direction and is the same in each cell. Inside the static field is a separate audio frequency $\cos\theta$ coil which provides a dressing field with amplitude of up to 100 μT oriented along the $\hat{x}$ direction. In between the static uniform field and the dressing field is a copper shield, which limits interaction between the dressing coil and the static field coil and acts as a flux return for the dressing field. To determine the relative phase between the neutron and ^{3}He spins, nEDM@SNS detects the spin-dependent capture rate of neutrons on ^{3}He through the reaction $\mathrm{n} + {}^3\mathrm{He} \rightarrow {}^3\mathrm{H} + p + 764$ keV. The critical dressing mode of the experiment uses a strong oscillating magnetic field to dress gyromagnetic ratios of neutrons and ^{3}He to the same value. This improves sensitivity to the nEDM by allowing continuous operation at the most sensitive relative phase between the neutron and ^{3}He [9] for a given ^{3}He concentration. However, this mode of measurement introduces additional noise, as current fluctuations in the spin dressing coil will lead to fluctuating magnetic fields. These fluctuating magnetic fields can cause the spins of neutrons and ^{3}He to drift apart over time.

Here, we use second-order time-dependent perturbation theory to assess the implications of magnetic field fluctuations for precision measurements performed on dressed spin

systems, with particular emphasis on applying these results to mitigate uncertainty in the critical dressing mode of the nEDM@SNS experiment. In Sec. II, we introduce the relevant Hamiltonian for spin dressing for a spin-1/2 system. In Sec. III, we apply time-dependent perturbation theory to this Hamiltonian to compute the phase variance, frequency shift, and run-to-run variance of the capture rate signal induced by a fluctuating dressing field. We express these results in terms of the power spectrum of these fluctuations. In this section, we also discuss the absence of run-to-run signal variance due to magnetic field gradients in either the static uniform field or the dressing field. In Sec. IV, we confirm these calculations by numerical integration of the Bloch equations, and discuss the implications of these results for the nEDM@SNS experiment. Section V proposes several strategies to mitigate dressing field fluctuations for the nEDM@SNS experiment. Finally, in Sec. VI, we introduce a modulation scheme which can be used to combat the dressing field noise addressed in the previous section, as well as enabling precise control of dressed spins in the presence of magnetic field gradients.

II. SPIN DRESSING HAMILTONIAN

A spin-1/2 system with gyromagnetic ratio γ precessing in a static uniform field $B_0\hat{z}$ and a strong oscillating magnetic dressing field $B_1\cos(\omega t)\hat{x}$ (with $B_1 > B_0$) is described by the Hamiltonian

$$H = \omega a^\dagger a + \frac{\Omega}{2}\sigma_x(a + a^\dagger) + \frac{\omega_0}{2}\sigma_z, \tag{1}$$

where σ_x, σ_y, and σ_z are the usual Pauli spin matrices, $a^\dagger$ and a are the raising and lowering operators for the photon field, $\omega_0 = \gamma B_0$ is the undressed frequency of a spin in a static uniform field, defined along $\hat{z}$, and Ω is a coupling constant given by

$$\Omega = \frac{\gamma B_1}{2\lambda^{1/2}}, \tag{2}$$

where $\lambda = \langle n\rangle$ is the average photon number. We are interested in how applying a small fluctuating magnetic field $\delta B(t)$ with a known power spectrum would affect the time evolution of an initial state $|\psi_0\rangle$ under this Hamiltonian.

III. THEORY

In the following section, we first outline a general framework to compute the expectation value and variance of operators under small, time-dependent perturbations to the Hamiltonian of Sec. II. We then use this framework to evaluate two observables to second order for a magnetic fluctuation $\delta B(t)$ which occurs parallel to the dressing field. These observables are the variance in phase for each spin species and the frequency shift for each spin species. For an experiment such as nEDM@SNS, these results can be used to estimate the sensitivity of dressed systems in the presence of field fluctuations. In deriving these formulas, we make no assumption about the source of the fluctuations, and therefore these results apply equally whether the random magnetic field arises from current fluctuations in the dressing coil or from static magnetic field gradients coupled with the stochastic motion of the spin species throughout the measurement cell. In the latter case, the power spectrum of $\delta B(t)$ may be calculated through the position-position autocorrelation function, as in [11]. In addition to these two observables, we also compute the variance of the phase between two species that are exposed to the same fluctuating magnetic field, as would be the case for current fluctuations. This is useful for nEDM@SNS, as the capture rate of neutrons on helium-3 depends linearly on this phase difference [9].

A. Time-dependent perturbation theory

Suppose that at time $t = 0$, a system is in the state $|\psi_0\rangle$, and we wish to compute the expectation value of some operator A_0 at some future time t. Given a time-dependent perturbation $V(t)$ to a Hamiltonian H, the time-evolution operator $T(t)$ to second order in time-dependent perturbation theory is given by

$$T(t) = 1 - i\int_0^t dt' V_I(t') - \int_0^t\int_0^{t'} dt'dt'' V_I(t')V_I(t'') + O(V^3), \tag{3}$$

where $V_I(t) \equiv e^{iHt}V(t)e^{-iHt}$ is the perturbation evaluated in the interaction picture. Thus, we need to compute $\langle\psi(t)|A_0|\psi(t)\rangle = \langle\psi_0|T(t)^\dagger A T(t)|\psi_0\rangle$, where A is likewise evaluated in the interaction picture, i.e., $A(t) \equiv e^{iHt}A_0e^{-iHt}$.

If $V(t)$ is proportional to $\delta B(t)$, then we can decompose $V_I(t)$ as a sum of complex exponentials as follows:

$$V_I(t) = \left(\sum_j Q_j e^{-i\omega_j t} + Q_j^\dagger e^{i\omega_j t}\right)\delta B(t), \tag{4}$$

where Q_j are time-independent operators. Provided that $\delta B(t)$ has zero mean, the terms of $T^\dagger A T$ which are linear in $\delta B(t)$ will vanish when we compute an expectation value over functions $\delta B(t)$. Therefore we need only consider the quadratic terms, which can be decomposed as

$$\sum_{j,k} f(Q_j, Q_k)\int_0^t dt'\int_0^{t'} dt'' e^{-i\omega_j t'}e^{i\omega_k t''}\delta B(t')\delta B(t''), \tag{5}$$

where $f(Q_j, Q_k)$ is some operator which is a function of only Q_j, Q_k, and their Hermitian conjugates. We now evaluate the expectation value of the integral over functions $\delta B(t)$,

$$\int_0^t dt'\int_0^{t'} dt'' e^{-i\omega_j t'}e^{i\omega_k t''}\langle\delta B(t')\delta B(t'')\rangle \tag{6}$$

$$= \int_0^t dt'\int_0^{t'} dt'' e^{-i(\omega_j-\omega_k)(t'+t'')/2}e^{-i(\omega_j+\omega_k)(t'-t'')/2}\langle\delta B(t')\delta B(t'')\rangle \tag{7}$$

$$= \frac{1}{2}\left(\int_0^{2t} d\bar{t} e^{-i\Delta\omega\bar{t}}\right)\left[\int_0^{t-|t-\bar{t}|} d\Delta t e^{-i\bar{\omega}\Delta t}\left\langle \delta B\left(\frac{\Delta t}{2}+\bar{t}\right)\delta B\left(-\frac{\Delta t}{2}+\bar{t}\right)\right\rangle\right] \tag{8}$$

$$\approx \frac{1}{2}\left(\int_0^{2t} d\bar{t} e^{-i\Delta\omega\bar{t}}\right)\left[\int_0^{\infty} d\Delta t e^{-i\bar{\omega}\Delta t} R_{\delta B}(\Delta t)\right], \tag{9}$$

where in Eq. (8) we have made the variable substitutions

$$\bar{\omega} \equiv \frac{\omega_1+\omega_2}{2}, \tag{10}$$

$$\Delta\omega \equiv \omega_1 - \omega_2, \tag{11}$$

$$\bar{t} = \frac{t'+t''}{2} \quad \text{(integration variable)}, \tag{12}$$

$$\Delta t = t' - t'' \quad \text{(integration variable)}, \tag{13}$$

$$R_{\delta B}(\Delta t) = \langle \delta B(\Delta t)\delta B(0)\rangle. \tag{14}$$

In Eq. (9), we assume that $\delta B(t)$ is stationary and has a short correlation time compared to t, and so it is valid to replace the limit of the second integral with infinity. The first integral in Eq. (9) only grows with time if $\Delta\omega \neq 0$, and therefore any term where $\Delta\omega \neq 0$ can be neglected. From this, we conclude that for the purpose of noise analysis, it is sufficient to consider the individual frequency components of $V_I(t)$ independently. Therefore, without loss of generality, we can write

$$V_I(t) = (Qe^{-i\omega t} + Q^\dagger e^{i\omega t})\delta B(t). \tag{15}$$

$T^\dagger A T$ can now be expressed in terms of Q and A to second order in V_I:

$$T^\dagger A T = A + \int_0^t\int_0^t dt' dt'' V_I(t'')AV_I(t') - \int_0^t dt'\int_0^{t'} dt'' V_I(t'')V_I(t')A + AV_I(t')V_I(t'') \tag{16}$$

$$= A + uu^*(QAQ^\dagger + Q^\dagger AQ) - v(Q^\dagger QA + AQQ^\dagger) - v^*(QQ^\dagger A + AQ^\dagger Q), \tag{17}$$

where we have defined the integrals

$$u(t;\omega) \equiv \int_0^t dt' e^{-i\omega t'}\delta B(t'), \tag{18}$$

$$v(t;\omega) \equiv \int_0^t dt'\int_0^{t'} dt'' e^{-i\omega(t'-t'')}\delta B(t')\delta B(t''). \tag{19}$$

We can further simplify Eq. (17) by noting that

$$v + v^* = \int_0^t dt'\int_0^{t'} dt''(e^{-i\omega\Delta t} + e^{+i\omega\Delta t})\delta B(t')\delta B(t'') \tag{20}$$

$$= \int_0^t\int_0^t dt' dt'' e^{-i\omega\Delta t}\delta B(t')\delta B(t'') \tag{21}$$

$$= uu^*. \tag{22}$$

If we now collect the terms proportional to v and v^*, we get

$$T^\dagger A T = A + [Q^\dagger,[A,Q]]v + [Q,[A,Q^\dagger]]v^*. \tag{23}$$

We can alternatively choose to collect terms proportional to $\mathrm{Re}(v)$ and $\mathrm{Im}(v)$, in which case we get

$$T^\dagger A T = A + ([Q,[A,Q^\dagger]] + [Q^\dagger,[A,Q]])\mathrm{Re}(v) + i[A,[Q^\dagger,Q]]\mathrm{Im}(v). \tag{24}$$

This allows us to calculate the expectation value of an operator A at time t in the interaction picture. In other cases, it may also be useful to calculate the variance of A. In the nEDM@SNS experiment, for example, variance in the capture rate signal, which depends linearly on the dot product between neutron and ^{3}He spins, could increase uncertainties in the nEDM measurement. In this particular case, we are concerned not with the quantum mechanical variance of $\vec{\sigma}_1\cdot\vec{\sigma}_2$ (which is nonzero even if the magnetic field has no fluctuations), but rather in how the magnetic field perturbs the spin vectors classically. In other words, we wish to find the variance of the quantum mechanical expectation value of $\vec{\sigma}_1\cdot\vec{\sigma}_2$. We thus define the classical variance of an operator A as

$$\mathrm{Var}_{cl}(A) \equiv \langle|\langle A\rangle|^2\rangle_{\delta B} - |\langle\langle A\rangle\rangle_{\delta B}|^2, \tag{25}$$

where $\langle\cdot\rangle_{\delta B}$ denotes an average over random functions $\delta B(t)$, while $\langle\cdot\rangle$ denotes a quantum mechanical expectation value, i.e., $\langle A\rangle \equiv \langle\psi|A|\psi\rangle$. A similar analysis as was used to derive Eq. (17) yields, in the case that A is Hermitian,

$$\mathrm{Var}_{cl}(T^\dagger A T) = 4\langle[Q^\dagger,A]\rangle\langle[A,Q]\rangle\mathrm{Re}(v). \tag{26}$$

These results can also be applied to a pair of noninteracting spin-1/2 systems through use of the tensor product. Suppose that in the interaction picture, the time-dependent perturbations for each of the two spins are given by

$$V_1(t) = (Q_1 e^{-i\omega t} + Q_1^\dagger e^{i\omega t})\delta B(t), \tag{27}$$

$$V_2(t) = (Q_2 e^{-i\omega t} + Q_2^\dagger e^{i\omega t})\delta B(t). \tag{28}$$

If we wish to compute the expectation value $\langle A\rangle$ from an initial state $|\psi\rangle_0 = |\psi_1\rangle_0 \otimes |\psi_2\rangle_0$, then we can apply Eq. (24) or (26) by substituting

$$Q \to Q_1\otimes I_2 + I_1\otimes Q_2, \tag{29}$$

where I_1 and I_2 are identity operators.

Lastly, we express v in terms of the power spectrum $S(\omega)$ of $\delta B(t)$. The power spectrum is defined as

$$S(\omega) \equiv \int_{-\infty}^{\infty} dt e^{-i\omega t} R_{\delta B}(t). \tag{30}$$

From Eq. (9), we have

$$v(t;\omega) = \frac{1}{2}\left(\int_0^{2t} d\bar{t}\right)\left[\int_0^{\infty} d\tau e^{-i\omega\tau} R_{\delta B}(\tau)\right] \tag{31}$$

$$= \frac{t}{2\pi}\int_0^{\infty} d\tau e^{-i\bar{\omega}\tau}\int_{-\infty}^{\infty} d\omega' S(\omega')e^{i\omega'\tau} \tag{32}$$

$$= \frac{t}{2\pi}\int_{-\infty}^{\infty} d\omega' S(\omega')\int_0^{\infty} d\tau e^{i(\omega'-\omega)\tau} \tag{33}$$

$$= \frac{t}{2\pi}\int_{-\infty}^{\infty} d\omega' S(\omega')\left[\pi\delta(\omega'-\omega) - \frac{i}{\omega'-\omega}\right] \tag{34}$$

$$= t\left[\frac{1}{2}S(\omega) - \frac{i}{2\pi}\int_{-\infty}^{\infty} d\omega' \frac{S(\omega')}{\omega'-\omega}\right]. \tag{35}$$

B. Initial state

An oscillating magnetic field corresponds quantum mechanically to a coherent state, denoted by $|\alpha\rangle$. A coherent state is an eigenstate of the lowering operator with eigenvalue α. The average photon number in such a state is given by $|\alpha|^2 = \lambda$, and so we separate α into its magnitude and complex phase as $\alpha \equiv \sqrt{\lambda}e^{i\theta}$. In the appendices, it is shown that a complex phase of α is equivalent to a rotation of the neutron and ^{3}He spins. The initial state in the following is taken to be

$$|\psi_0\rangle = |\alpha\rangle\,|s\rangle\,, \tag{36}$$

where $|s\rangle$ is the initial spin state, or if we are considering both the neutron and ^{3}He spins,

$$|\psi_0\rangle = |\alpha\rangle\,|s_1\rangle\,|s_2\rangle\,. \tag{37}$$

C. Computation of matrix elements

We now compute the Q operators [and thus $V_I(t)$] for the spin dressing Hamiltonian in the case where the time-dependent fluctuating magnetic field is parallel to $\hat{x}$. This calculation will proceed in two steps. We first apply a carefully chosen time-independent unitary transform to the Hamiltonian in order to compute its eigenstates, and then compute the matrix elements of the operator σ_x with respect to these states. We then transform these matrix elements into the interaction picture by multiplying each matrix element by the appropriate time-dependent phase factor. In the limit where $\lambda \gg 1$ and $\omega \gg \omega_0$, the eigenstates and eigenvalues of the spin dressing Hamiltonian can be approximately found by expressing H as $H = H_0 + H_z$, where

$$H_0 = \omega a^\dagger a + \frac{\Omega}{2}\sigma_x(a + a^\dagger), \tag{38}$$

$$H_z = \frac{\omega_0}{2}\sigma_z. \tag{39}$$

As shown in [1], H_0 can be diagonalized by considering each of the two eigensubspaces of σ_x individually. The Hamiltonians of the two subspaces are given by

$$H_\epsilon = \omega a^\dagger a + \frac{\Omega}{2}\epsilon(a + a^\dagger), \tag{40}$$

where $\epsilon \in \{1, -1\}$ corresponds to the eigenvalues of σ_x. The part of the Hamiltonian contained in H_ϵ is diagonalized by applying the displacement operator $D(\epsilon\Omega/2\omega)$, which is defined by its action on the raising and lower operators:

$$D^\dagger(\eta) a D(\eta) \equiv a + \eta, \tag{41}$$

$$D^\dagger(\eta) = D(-\eta). \tag{42}$$

Explicitly, the displacement operator is given by

$$D(\eta) \equiv e^{\eta a^\dagger - \eta^* a}. \tag{43}$$

Note that while the definition of the displacement operator $D(\eta)$ allows for complex η, here we restrict our attention to the case where η is real. Applying this operator to H_ϵ and abbreviating $D(\epsilon\Omega/2\omega)$ as D_ϵ yields

$$D_\epsilon H_\epsilon D_\epsilon^\dagger = \omega D_\epsilon a^\dagger a D_\epsilon^\dagger + \frac{\epsilon\Omega}{2} D_\epsilon (a + a^\dagger) D_\epsilon^\dagger \tag{44}$$

$$= \omega\left(a^\dagger - \frac{\epsilon\Omega}{2\omega}\right)\left(a - \frac{\epsilon\Omega}{2\omega}\right) + \frac{\epsilon\Omega}{2}\left(a + a^\dagger - \frac{\epsilon\Omega}{\omega}\right) \tag{45}$$

$$= \omega a^\dagger a - \frac{\Omega^2}{4\omega}. \tag{46}$$

From D_ϵ, we can construct a unitary operator U, which applies D_ϵ to the appropriate eigensubspace of σ_x. Explicitly,

$$U \equiv D\left(\frac{\Omega}{2\omega}\right)|+_x\rangle\langle+_x| + D^\dagger\left(\frac{\Omega}{2\omega}\right)|-_x\rangle\langle-_x|\,, \tag{47}$$

where $|\pm_x\rangle$ are the eigenvectors of σ_x. Applying U to H_0 yields

$$U H_0 U^\dagger = \omega a^\dagger a - \frac{\Omega^2}{4\omega}. \tag{48}$$

We thus see that U diagonalizes H_0, and that the eigenstates of $U H_0 U^\dagger$ are $|n\rangle\,|\pm_z\rangle$. Meanwhile, H_z in this basis becomes

$$U H_z U^\dagger = \frac{\omega_0}{2}\left[D^\dagger\left(\frac{\Omega}{\omega}\right)|+_x\rangle\langle-_x| + D\left(\frac{\Omega}{\omega}\right)|-_x\rangle\langle+_x|\right]. \tag{49}$$

For large photon number ($\lambda \gg 1$), the displacement operator can be approximated in terms of Bessel functions. Reference [1] gives the matrix elements of $D(\eta)$ as

$$\langle n|\,D(\eta)\,|n-q\rangle = \langle n|\,e^{\eta(a^\dagger - a)}\,|n-q\rangle = J_q(2\eta\sqrt{\lambda}), \tag{50}$$

where J_q is a Bessel function of the first kind with order q. From this, we derive

$$D(\eta) \approx \sum_{n,q} J_q(2\eta\sqrt{\lambda})\,|n+q\rangle\langle n|\,. \tag{51}$$

With this approximation, the full Hamiltonian H in the displaced basis is

$$U H U^\dagger = \omega a^\dagger a + \frac{\omega_0}{2}J_0(x)\sigma_z - \frac{\omega_0}{2}J_1(x)\left(\sum_n |n\rangle\langle n+1| - |n+1\rangle\langle n|\right)i\sigma_y + \frac{\omega_0}{2}J_2(x)\left(\sum_n |n\rangle\langle n+2| + |n+2\rangle\langle n|\right)\sigma_z + O(q \geqslant 3), \tag{52}$$

where we have defined the spin dressing parameter $x \equiv 2\Omega\sqrt{\lambda}/\omega = \gamma B_1/\omega$. In Ref. [3], the matrix elements of various perturbations are calculated in time-dependent perturbation theory. Here, we extend those results to the case where ω_0 may not be small compared to ω by incorporating

the first-order correction to the eigenstates of $UH_0U^\dagger$. We first consider the energy correction. Let the eigenstates of $UHU^\dagger$ be denoted by $\widetilde{|n,\pm_z\rangle}$. Treating H_z as a perturbation on H_0, the energies of these states can be calculated to first order in ω_0/ω using perturbation theory, as in Ref. [1]. The energy shift is simply

$$E_{n,\pm} = E^{(0)}_{n,\pm} + \langle n|\langle \pm_z| H_z |\pm_z\rangle |n\rangle \tag{53}$$

$$= n\omega \pm \frac{\omega_0}{2} J_0(x). \tag{54}$$

H_z thus lifts the degeneracy of $|n\rangle|\pm_z\rangle$ and leads to an effective Larmor frequency $\omega_0' \equiv \omega_0 J_0(x)$. We similarly derive the eigenstates of $UHU^\dagger$ to first order in ω_0/ω:

$$\widetilde{|n,\pm_z\rangle} = |n\rangle|\pm_z\rangle \pm \frac{J_1(x)\omega_0}{2\omega}(|n-1\rangle|\mp_z\rangle + |n+1\rangle|\mp_z\rangle) \pm \frac{J_2(x)\omega_0}{4\omega}(|n-2\rangle|\pm_z\rangle - |n+2\rangle|\pm_z\rangle) + O(q\geqslant 3). \tag{55}$$

We can now calculate the matrix elements of various time-dependent perturbations with respect to these eigenstates. For dressing field noise generated from fluctuations in the current provided by the power supply, the only relevant operator is σ_x, provided the linearly polarized dressing field is homogeneous. Fortunately, σ_x is unchanged by U, as $U\sigma_x U^\dagger = \sigma_x$. We obtain

$$\widetilde{\langle n,\pm_z|}\sigma_x\widetilde{|n',\pm_z\rangle} = \pm\frac{J_1(x)\omega_0}{\omega}\delta_{1,|n-n'|} + O(q\geqslant 3), \tag{56}$$

$$\widetilde{\langle n,\pm_z|}\sigma_x\widetilde{|n',\mp_z\rangle} = \delta_{n,n'} \pm \frac{J_2(x)\omega_0}{2\omega}\delta_{2,|n-n'|} + O(q\geqslant 3). \tag{57}$$

We have truncated terms containing Bessel functions of order 3 or greater. From these matrix elements, we can now evaluate the perturbation in the interaction picture by computing the individual frequency components of $e^{iUHU^\dagger t}\sigma_x e^{-iUHU^\dagger t}$ using

$$e^{iUHU^\dagger t} = \sum_{n,s} \widetilde{|n,s\rangle}\widetilde{\langle n,s|} e^{i\omega_{n,s}t}, \tag{58}$$

where $\hbar\omega_{n,s}$ is the energy of the state $\widetilde{|n,s\rangle}$. Expanding $e^{iUHU^\dagger t}\sigma_x e^{-iUHU^\dagger t}$, we get

$$e^{iUHU^\dagger t}\sigma_x e^{-iUHU^\dagger t} = \sum_{n,n',s,s'} \widetilde{|n,s\rangle}\widetilde{\langle n,s|}\sigma_x\widetilde{|n',s'\rangle}\widetilde{\langle n',s'|} e^{i\Delta\omega t}, \tag{59}$$

where $\Delta\omega$ is the frequency difference between $\widetilde{|n,s\rangle}$ and $\widetilde{|n',s'\rangle}$. Here we only consider the leading-order term of each frequency component, so we make the approximation that $\widetilde{|n,s\rangle}\widetilde{\langle n',s'|} \approx |n\rangle|s\rangle\langle n'|\langle s'|$. With this approximation, we can now write

$$e^{iUHU^\dagger t}\sigma_x e^{-iUHU^\dagger t} = W + W^\dagger, \tag{60}$$

where

$$W = -\sigma_- e^{-i\omega_0' t} + \sigma_z \sum_n |n-1\rangle\langle n| \frac{J_1(x)\omega_0}{\omega} e^{-i\omega t} - \sigma_- \sum_n |n-2\rangle\langle n| \frac{J_2(x)\omega_0}{2\omega}\left(e^{-i(2w+\omega_0')t} - e^{-i(2w-\omega_0')t}\right) + O(q\geqslant 3). \tag{61}$$

We can simplify this expression further. In the classical limit, we can make the approximation that

$$a \approx \sqrt{\lambda}\sum_n |n-1\rangle\langle n|, \tag{62}$$

provided that λ is large. Thus, when applying operators of the form $\sum_n |n-q\rangle\langle n|$ to a coherent state, we get

$$\left(\sum_n |n-q\rangle\langle n|\right)|\alpha\rangle \approx \frac{a^q}{\sqrt{\lambda^q}}|\alpha\rangle \tag{63}$$

$$= e^{iq\theta}|\alpha\rangle. \tag{64}$$

This allows us to replace the terms operating on the photon field in W with simple phase factors. Thus,

$$W = -\sigma_- e^{-i\omega_0' t} + \sigma_z e^{i\theta}\frac{J_1(x)\omega_0}{\omega} e^{-i\omega t} - \sigma_- e^{2i\theta}\frac{J_2(x)\omega_0}{2\omega}(e^{-i(2w+\omega_0')t} - e^{-i(2w-\omega_0')t}) + O(q\geqslant 3). \tag{65}$$

Each independent frequency term of W corresponds to a Q operator. In particular, for a perturbation $\delta H(t) = \sigma_x \delta B(t)$, the corresponding Q operators are

$$Q_{\omega_0'} = -\sigma_-, \tag{66}$$

$$Q_\omega = \frac{J_1(x)\omega_0}{\omega}\sigma_z, \tag{67}$$

$$Q_{2\omega+\omega_0'} = -\frac{J_2(x)\omega_0}{2\omega}\sigma_-, \tag{68}$$

$$Q_{2\omega-\omega_0'} = \frac{J_2(x)\omega_0}{2\omega}\sigma_+. \tag{69}$$

In writing these operators, we have omitted any phase factors, as in both Eqs. (24) and (26), Q is always paired with $Q^\dagger$ and so any phase factor will be eliminated.

D. Explicit calculation for magnetic field fluctuations

Recalling that Eq. (24) allows us to calculate the expectation value of an operator at any time in the interaction picture, and combining Eqs. (24) and (66)–(69), we can now explicitly compute the effects of fluctuations in the amplitude and phase of the dressing field. As in [3], we compute the phase variance and frequency shifts by taking the real and imaginary parts of $\langle\sigma_x + i\sigma_y\rangle$ in the interaction picture (rotating frame) for a spin which starts in the $+\hat{x}$ direction at time $t = 0$, i.e., $|\psi_0\rangle = (|+_z\rangle + |-_z\rangle)/\sqrt{2}$. We will denote the rate of accumulation

of phase variance as Γ_ϕ and the frequency shift as $\delta\omega$. Given a perturbation $\delta H(t) = \gamma \delta B(t)\sigma_x/2$, we obtain

$$\Gamma_\phi = -\frac{d\langle\sigma_x\rangle}{dt} = \frac{\gamma^2}{4}S(\omega_0') + \left(\frac{\gamma J_1(x)\omega_0}{\omega}\right)^2 S(\omega) + \frac{1}{4}\left(\frac{\gamma J_2(x)\omega_0}{2\omega}\right)^2 [S(2\omega-\omega_0') + S(2\omega+\omega_0')] + O(q \geqslant 3), \tag{70}$$

$$\delta\omega = \frac{d\langle\sigma_y\rangle}{dt} = -\frac{\gamma^2}{4\pi}\int_{-\infty}^{\infty} d\omega' \frac{S(\omega')}{\omega'-\omega_0'} - \frac{1}{4\pi}\left[\frac{\gamma J_2(x)\omega_0}{2\omega}\right]^2 \int_{-\infty}^{\infty} d\omega' S(\omega') \times \left(\frac{1}{\omega'-2\omega+\omega_0'} + \frac{1}{\omega'-2\omega-\omega_0'}\right) + O(q \geqslant 3). \tag{71}$$

We note that in the case where $\delta B(t)$ is different for spins in the same measurement cell, as would be the case for magnetic field gradients, Γ_ϕ may be regarded as the transverse relaxation rate, i.e., $\Gamma_\phi = 1/T_2$. Conversely, in the case where all neutrons experience the same time-dependent magnetic field as would be the case for dressing field fluctuations arising due to current fluctuations in the dressing coil, Γ_ϕ represents the run-to-run phase variation. That is, $\Gamma_\phi = \frac{d}{dt}\mathrm{Var}(\phi)$, where the variance is taken over multiple runs of the experiment. While Γ_ϕ and $\delta\omega$ are quantities that are of general importance in situations where precise control of the phase of dressed spins is required, for nEDM@SNS we are particularly concerned with effects which can perturb the neutron-^{3}He capture rate. This rate depends linearly on $\vec{\sigma}_1 \cdot \vec{\sigma}_2$, so we would like to compute the variance of this operator in order to find the run-to-run variance in the signal rate, this time under the assumption that the neutrons and ^{3}He atoms are exposed to the same magnetic field. However, the expectation values computed from time-dependent perturbation theory are in the interaction picture, so to convert these values to those actually observed in the laboratory frame we must find the variance of $U_1 U_2 e^{iHt}\sigma_1 \cdot \sigma_2 e^{-iHt} U_2^\dagger U_1^\dagger$. Details of this calculation are found in Appendix D. Generically, this is a time-dependent operator having terms which oscillate at frequencies that are sums of integer multiples of the dressing field frequency ω and the dressed Larmor precession frequency ω_0'. However, because capture signal rates in the nEDM@SNS experiment are not sufficiently high to resolve oscillations at these frequencies, we consider only the time-independent component of this operator. We can now calculate the variance in the capture rate due to a fluctuating magnetic field. Let $\vec{b}_1 = \langle\vec{\sigma}_1\rangle(t=0)$ and $\vec{b}_2 = \langle\vec{\sigma}_2\rangle(t=0)$ be the Bloch vectors of the neutron and ^{3}He atom at time $t = 0$. Then,

$$\mathrm{Var}_{cl}(\sigma_1\cdot\sigma_2)(t) = \frac{1}{2}(\gamma_1-\gamma_2)^2|\hat{z}\times(\vec{b}_1\times\vec{b}_2)|^2 S(\omega_0')t + 2\left(\frac{\gamma_1 J_1(x_1)\omega_1 - \gamma_2 J_1(x_2)\omega_2}{\omega}\right)^2 |\hat{z}\cdot(\vec{b}_1\times\vec{b}_2)|^2 S(\omega)t + \frac{1}{2}\left(\frac{\gamma_1 J_2(x_1)\omega_1 - \gamma_2 J_2(x_2)\omega_2}{2\omega}\right)^2 |\hat{z}\times(\vec{b}_1\times\vec{b}_2)|^2 [S(2\omega-\omega_0') + S(2\omega+\omega_0')]t + O(q\geqslant 3). \tag{72}$$

The first term in Eq. (72) represents the variance due to noise at the effective Larmor frequency. However, if both spins start in the plane of precession, this term will not contribute. The second term represents variance due to noise at the dressing frequency, which unlike the first term is maximized if the spins start in the plane of precession. The third term, like the first, is minimized when the spins start in the plane of the precession and is generated from noise at twice the dressing frequency shifted by the effective Larmor precession frequency.

Equation (72) may appear to suggest that if $\vec{b}_1 = \vec{b}_2$, one could altogether eliminate variance due to current fluctuations. However, under critical spin dressing, the quantity proportional to the nEDM is the relative phase between neutron and ^{3}He spins, i.e., $\phi_2 - \phi_1 \propto d_n$. Meanwhile, the signal rate of nEDM@SNS is linear in $\sigma_1\cdot\sigma_2$, which is in turn related to the relative phase by

$$\sigma_1\cdot\sigma_2 = \cos(\phi_2-\phi_1), \tag{73}$$

provided both spins start in the plane of precession. Thus, setting $\phi_2 = \phi_1$ would decrease sensitivity to an nEDM, as $\sigma_1\cdot\sigma_2$ would no longer be sensitive to the relative phase in this configuration. Furthermore, the variance of $\phi_2 - \phi_1$ is independent of the starting phase of either spin. Again, assuming both spins start in the plane of precession,

$$\hat{z}\cdot(\vec{b}_1\times\vec{b}_2) = \sin(\phi_2-\phi_1). \tag{74}$$

The variance can be propagated using the Taylor expansion. We have

$$\mathrm{Var}_{cl}(\sigma_1\cdot\sigma_2) \approx |\sin(\phi_2-\phi_1)|^2 \mathrm{Var}_{cl}(\phi_2-\phi_1). \tag{75}$$

Therefore, in the plane of precession, the phase of the spin of one species with respect to the other spin species does not matter, and the variance in the relative phase will accumulate according to

$$\mathrm{Var}_{cl}(\phi_2-\phi_1) \approx 2\left(\frac{\gamma_1 J_1(x_1)\omega_1 - \gamma_2 J_1(x_2)\omega_2}{\omega}\right)^2 S(\omega)t. \tag{76}$$

In Fig. 1, we show the per-run frequency uncertainty due to noise in the dressing field with a perfect band pass around the dressing frequency, predicted by Eq. (76). Explicitly, the frequency uncertainty is found by taking the square root of the variance at a given time in the measurement to find the standard deviation of the phase at that time, then dividing this phase uncertainty by the time in the measurement to find the frequency uncertainty. The per-run sensitivity of

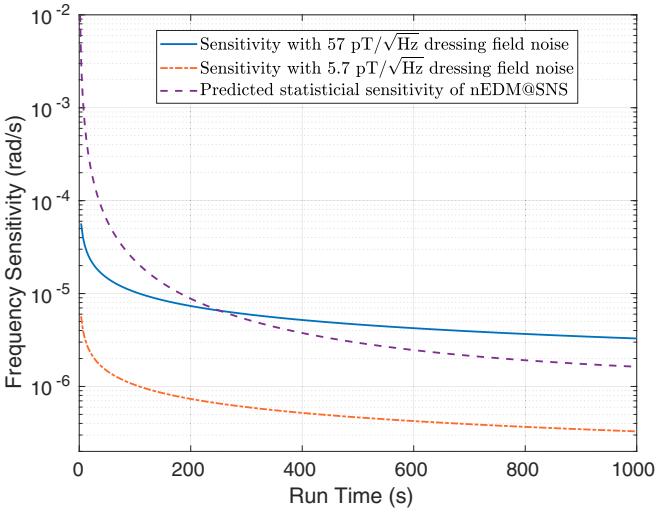

FIG. 1. Run-to-run uncertainty in the measured frequency due to dressing field noise for 57 and 5.7 pT/$\sqrt{\text{Hz}}$ dressing field noise and a perfect band-pass filter around the dressing frequency, calculated from Eq. (76). The predicted per-run sensitivity for the nEDM@SNS, formulated from Ref. [9], is shown for comparison. It is shown that 57 pT/$\sqrt{\text{Hz}}$ dressing field noise will significantly reduce the ultimate sensitivity of the measured frequency, while 5.7 pT/$\sqrt{\text{Hz}}$ dressing field noise is acceptable.

nEDM@SNS according to Ref. [9] is also shown for comparison. If we define. the signal-to-noise ratio (SNR) to be

$$\text{SNR} = P_{\text{signal}}/P_{\text{noise}} = (A_{\text{signal}}/A_{\text{noise}})^2, \tag{77}$$

where P is the power of the signal or noise and A is the corresponding amplitude, we find that for 80 dB SNR, and a perfect band-pass filter around the dressing frequency, the phase uncertainty is comparable in magnitude to the statistical sensitivity of nEDM@SNS.

Lastly, we find an absence of run-to-run signal variance for neutrons and ^{3}He, $\text{Var}_{cl}(\sigma_n \cdot \sigma_3)$, from magnetic fluctuations arising from motion in a static magnetic gradient of any field along any direction, assuming that the gradient field does not change from run to run. This is due to two effects: first, for each run, $\sigma_n \cdot \sigma_3$ is averaged over many particles as each neutron and ^{3}He samples a different magnetic field; and second, the neutron and ^{3}He trajectories are uncorrelated, and so Eq. (72) (which is derived under the assumption that the neutron and ^{3}He are exposed to the same field) does not apply. Instead, because these trajectories are uncorrelated, the decay rate of the signal during a run can be computed from the relaxation rate of each individual species using the formalism of Ref. [3]. The relaxation rate and frequency shifts for each species are given by the expectation value of σ_+,

$$\text{Re}(\langle\sigma_+\rangle) = 1 - \frac{t}{T_2}, \tag{78}$$

$$\text{Im}(\langle\sigma_+\rangle) = \delta\omega t. \tag{79}$$

Therefore, keeping only terms to second order in magnetic gradients after computing the expectation value of σ_+ and σ_z with the perturbed wave function, we find

$$\text{Re}(\langle\sigma_{+_n}\rangle\langle\sigma_{-_3}\rangle) = 1 - \frac{t}{T_{2_n}} - \frac{t}{T_{2_3}}, \tag{80}$$

$$\langle\sigma_{z_n}\rangle\langle\sigma_{z_3}\rangle \approx 0. \tag{81}$$

Using the identity $\sigma_n \cdot \sigma_3 = \sigma_{z_n}\sigma_{z_3} + \text{Re}(\sigma_{+_n}\sigma_{-_3})$, we derive

$$\frac{d\langle\sigma_n \cdot \sigma_3\rangle}{dt}\frac{1}{\cos(\phi_n - \phi_3)} = -\left(\frac{1}{T_{2_n}} + \frac{1}{T_{2_3}}\right) \approx -\frac{1}{T_{2_3}}. \tag{82}$$

The transverse relaxation T_2 for both species can be calculated from Ref. [3]. Typically, because the trajectories of UCN are ballistic, and highly oscillatory in the measurement cell resulting in significant motional narrowing, the contribution of the transverse relaxation of the neutron to the signal decay is small. This result shows that there is no run-to-run phase fluctuation if the gradients of all magnetic fields remain the same, run to run. The gradients in the magnetic fields diminish the statistical sensitivity by decreasing the coherence time of a single measurement, and the effect is predictable without stochastic variations, contrary to the case with dressing field amplitude fluctuations.

TABLE I. Optimized parameters for the starting position on the Bloch sphere for neutrons and ^{3}He to achieve cosine dressing with a sine dressing field described in Sec. III E. $\phi_{n3} = \phi_n - \phi_3$ is the relative azimuthal angle of the neutron and ^{3}He that is desired during critical dressing; $\phi_{n,3}$ and $\theta_{n,3}$ are the absolute azimuthal angle and absolute polar angle of the neutron and ^{3}He, respectively. When the neutron and ^{3}He start at these positions with sine dressing, the result is cosine dressing dynamics for the respective relative phase ϕ_{n3}. All units are in radians. Values are for the fiducial nEDM@SNS experiment parameters for critical dressing, where the dressing field amplitude is 40.2497 μT oscillating at 1 kHz with a static uniform field strength of 5.2 μT in the $\hat{z}$ direction. Optimization of the fiducial nEDM@SNS parameters is discussed in Ref. [9].

ϕ_{n3}	ϕ_n	θ_n	ϕ_3	θ_3
0	−0.99650	1.81020	−1.00759	1.85511
$\pi/4$	−0.59186	1.84162	−1.40374	1.77373
$\pi/2$	−0.18485	1.83092	−1.78485	1.66284

E. The feasibility of dressing with a cosine wave form

In order to minimize the variance in Eq. (72), both spins should start in the plane of precession at $t = 0$. However, in deriving Eq. (72), we assumed a magnetic field with a cosine dependence, i.e., $B_x(t) = B_1\cos(\omega t)$. This poses a problem, as such a dressing pulse would require an instantaneous change in magnetic field at $t = 0$, which is impossible to achieve due to the inductance of the dressing coil and limited slew rates of power supplies. Instead, the same dynamics can be achieved with sine dressing, i.e., $B_x(t) = B_1\sin(\omega t)$, by having the neutron and ^{3}He spins start outside the plane of precession. The polar angle $\theta_{n,3}$ and absolute phase $\phi_{n,3}$ of the neutron and ^{3}He required at $t = 0$ to achieve this are specified in Table I.

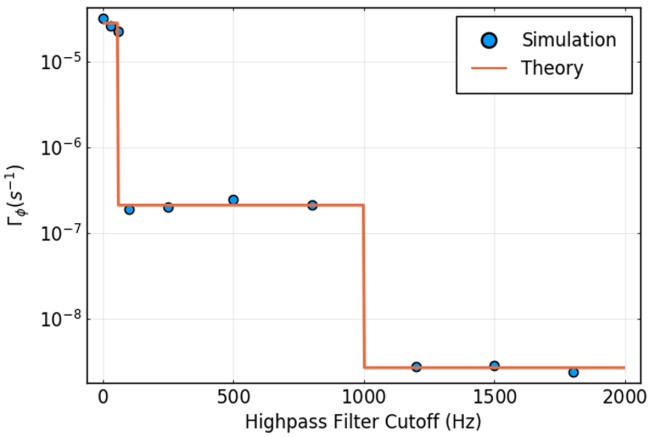

FIG. 2. Predicted and simulated values of Γ_ϕ for various high-pass filter cutoffs. The theory line is calculated from Eqs. (70) and (83). Each simulated point represents 200 neutrons. Note that cutoff values beyond the dressing frequency (1000 Hz) are only achievable in simulation, and are shown here for comparison to the theory.

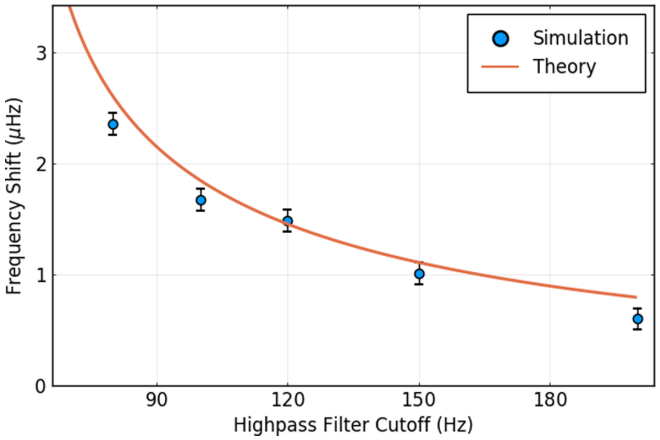

FIG. 3. Predicted and simulated frequency shifts, with magnetic field noise given by Eq. (83), for various high-pass filter cutoffs. The theory line is calculated from Eqs. (71) and (83). Each simulated point represents 100 000 neutrons.

IV. SIMULATION

The calculations in the previous section are verified by numerically integrating the Bloch equations with an adaptive Runge-Kutta integrator. Ensembles of spins are simulated using the fiducial critical spin dressing parameters for the nEDM@SNS experiment ($B_1 \approx 40\ \mu$T, $\omega \approx 2\pi \times 1$ kHz, $\omega_0' \approx 2\pi \times 100$ Hz), with the addition of a noisy magnetic field with amplitude spectral density of $57\,\mathrm{pT}/\sqrt{\mathrm{Hz}}$. This assumed spectral density corresponds to a 0.01% rms variation in B_1 over a bandwidth of 5 kHz. While this is a reasonable figure for the power supplies being considered for nEDM@SNS, it should be noted that the noise power spectrum for the dressing field will generally be peaked around the dressing field frequency, and therefore $S(\omega = 1\,\mathrm{kHz})$ may be significantly larger than the assumed value of $57\,\mathrm{pT}/\sqrt{\mathrm{Hz}}$. The noise power spectrum is varied by changing the cutoff frequency of a simulated high-pass filter. In computing the theoretical values, we assume that this high-pass filter is ideal, so that

$$S(\omega) = \begin{cases} (57\,\mathrm{pT}/\sqrt{\mathrm{Hz}})^2, & |\omega| > \omega_{\mathrm{cutoff}} \\ 0 & \text{otherwise.} \end{cases} \tag{83}$$

We substitute this power spectrum into Eqs. (70) and (71) to obtain the theory line in Figs. 2 and 3. Figure 2 shows the simulated and theoretical relaxation times for different values of the high-pass filter cutoff. As evidenced by a sharp decrease in relaxation rate as the cutoff frequency is swept past $2\pi\omega_0'$ and $2\pi\omega$, T_2 depends only on the power spectral density at a set of discrete frequencies. Figure 3 compares the simulated and theoretical frequency shifts. The frequency shift decreases logarithmically as the high-pass filter cutoff is increased past the dressed Larmor frequency. Therefore, if a physical high-pass filter is employed to reduce the run-to-run phase variation due to current fluctuations, its cutoff frequency should be chosen to be well above the Larmor frequency in order to mitigate the frequency shift. It should be noted, however, that for the case of nEDM@SNS experiment, a frequency shift caused by current fluctuations can be corrected for by comparing the signal from the two measurement cells for the same run or by comparing the signal after reversal of the electric field.

A. Discussion of results

The results derived in Sec. III and verified in Sec. IV apply generally to any time-dependent magnetic field perturbation parallel to the dressing field. For nEDM@SNS, these perturbations can arise primarily from two sources: current fluctuations in the dressing coil, or gradients in the magnetic field coupled with the random motion of neutrons and ^{3}He atoms in the measurement cells. We first consider the case of current fluctuations, in which all spins are exposed to the same fluctuating magnetic field. As shown in Figs. 2 and 3, the effect of these fluctuations can be separated into two components: the run-to-run variation in phase caused by the stochastic nature of the fluctuations, and a systematic frequency shift. The frequency shift is relatively harmless for nEDM@SNS, as this shift is eliminated by reversal of the electric field. However, the variation in phase over the course of multiple runs can pose a problem, as this contributes directly to the statistical uncertainty of the nEDM measurement, as evidenced by Fig. 1. Because the phase accumulated by this effect varies from run to run, electric field reversal will not nullify this effect. One could also attempt to correlate the scintillation signals from each of the two measurement cells under the assumption that the perturbing magnetic field is identical between the two cells. However, this approach also has limitations, as we discuss in the following section. Especially problematic is noise at the dressing field frequency, as the results of Eq. (72) indicate that the primary contribution to phase variance for spins precessing in the plane orthogonal to the static field comes from noise at this frequency. This is compounded with the results from tests with the power supply used in Sec. V B, which indicate that the noise power spectrum is peaked around the dressing field frequency. Thus, to reduce the statistical uncertainty caused by fluctuations in the dressing field, the following section will explore several techniques to mitigate this type of noise.

V. MITIGATION STRATEGIES

The considerations in the previous sections show that fluctuations in the nEDM signal due to current fluctuations in the dressing coil would arise primarily due to the noise power spectrum at $S(\omega)$, which corresponds to amplitude fluctuations in the dressing field. We discuss two strategies to mitigate this effect. First, one can leverage the fact that the two measurement cells of nEDM@SNS are exposed to opposite electric fields in order to eliminate this effect during data postprocessing; however, as we show, this approach has limitations when there are static field gradients between the two cells. An alternative approach is to directly reduce $S(\omega)$ by applying feedback to the dressing coil in order to maintain the dressing field amplitude close to its target value.

A. Cross-cell correlation

In order to combat systematic effects, the nEDM@SNS experiment uses two measurement cells which will be exposed to opposite electric fields [9]. Under the assumption that the magnetic field noise $\delta B(t)$ is identical in the two cells, it may be possible to correlate the effects of dressing field noise in the two cells and thus eliminate its effect on the measurement of the neutron EDM. One confounding factor for this strategy is the presence of static magnetic field gradients. Due to imperfections in the static and dressing field coils, the dressed Larmor frequencies between the two cells may differ by a small amount. In this case, the same noise field $\delta B(t)$ may affect the two cells differently, hampering our ability to correlate the two cells. In order to determine the correlations between the spins in different cells, we compute the expectation value $\langle \vec{\sigma}_1 \cdot \vec{\sigma}_2 \rangle$, where $\vec{\sigma}_1$ and $\vec{\sigma}_2$ represent two spins of the same species in opposite cells. Let ω_1 and ω_2 be the dressed Larmor frequencies in the two cells. In this case, calculating the expectation value is complicated by the fact that ω_1 and ω_2 may be very close in frequency, and thus we can no longer use the approximation that cross-frequency terms may be neglected. These terms are calculated in Appendix A. The expectation value $\langle \vec{\sigma}_1 \cdot \vec{\sigma}_2 \rangle$ is then given by

$$\langle \vec{\sigma}_1 \cdot \vec{\sigma}_2 \rangle = 1 - \frac{\gamma^2}{2} S(\bar{\omega}) \left(t - \frac{\sin(2\Delta\omega t)}{2\Delta\omega} \right). \tag{84}$$

We see that decorrelation between the two cells may only be neglected if either $S(\bar{\omega})$ is small or $\Delta\omega t$ remains small over the course of the experiment.

B. Feedback control

In situations where decorrelation between the two cells is too large to apply the strategy of the previous section, we can instead employ feedback control on the dressing field. As we are primarily concerned with amplitude fluctuations in the dressing field, we regard the instantaneous dressing amplitude as a constant ideal value, $B_{1,\text{ideal}}$, plus a small fluctuating $\delta B_1(t)$, so that the dressing field is given by $B(t) = [B_{1,\text{ideal}} + \delta B_1(t)] \cos(\omega t)$. Under critical dressing, the phase accumulated between the neutron and ^{3}He is, to first order in $\delta B_1(t)$, proportional to the integral of $\delta B_1(t)$ over time. Thus, one way to limit the impact of current fluctuations would be to employ feedback control to minimize the deviation of this integral from a target value. Using a Kepco four-quadrant 400 36-12 power supply and a DT9837A digital signal analyzer, we demonstrate a proof of concept for using feedback control in the nEDM@SNS experiment. The signal analyzer outputs a 1000 Hz sine wave, which we feed into the voltage control input of the power supply. The power supply drives a cosine coil, at the center of which is a pickup coil. The voltage across this pickup coil is measured by the signal analyzer, and the output of the signal analyzer is adjusted based on this measurement using a digital PI loop to maintain the integral of the signal amplitude near its target value. We then use the measured fluctuating magnetic field to simulate the motion of neutron and ^{3}He spins, using the CODATA values for their gyromagnetic ratios [12]. The measured magnetic field is postprocessed with a high-pass filter to remove lower-frequency noise, and a single global scaling factor is applied to the field to replicate the CSD parameters of the nEDM@SNS experiment. Figures 4 and 5 show the resulting rms deviation of the relative phase shift between neutron and ^{3}He spins. In Fig. 5, we also plot the phase accumulation estimated by applying Eq. (76) to the measured noise power spectrum of the Kepco power supply. Assuming a 400 pT/$\sqrt{\text{Hz}}$ white noise spectrum which is then high-pass filtered at 500 Hz, we can see that this approach underestimates the actual phase accumulation. This indicates that, as expected, the noise power spectrum is peaked around the dressing field frequency. Nonetheless, these results show that introducing the feedback loop substantially reduces the run-to-run phase variation caused by amplitude fluctuations in the dressing field. There are a number of ways to implement this type of feedback loop in the nEDM@SNS experiment. A simple scheme would be to place a shunt resistor in series with the dressing coil to measure the current. Alternatively, pickup coils may be used, as was done in this section. The advantage of this approach for nEDM@SNS is that multiple pickup coils can be used to detect spatial inhomogeneities in the dressing field. This latter approach also enables us to detect changes in

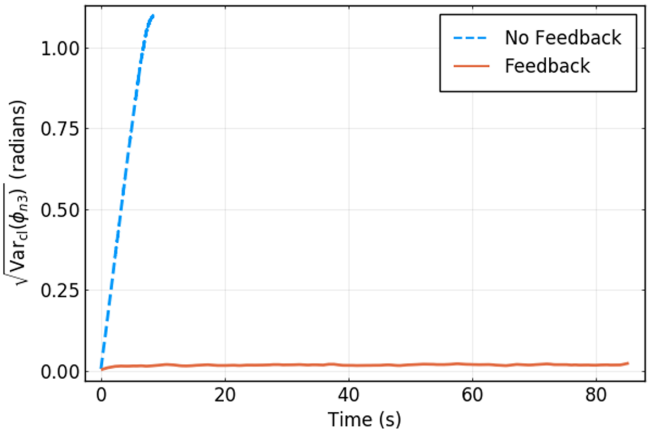

FIG. 4. The root-mean-square deviation of the angle between the neutron and ^{3}He spins (ϕ_{n3}) as a function of time, with dressing field powered by a Kepco four-quadrant 400 36-12 power supply, for magnetic fields generated with (solid line) and without (dashed line) feedback control. The dataset without feedback consists of 28 runs, while the dataset with feedback consists of 50. Data are smoothed for clarity.

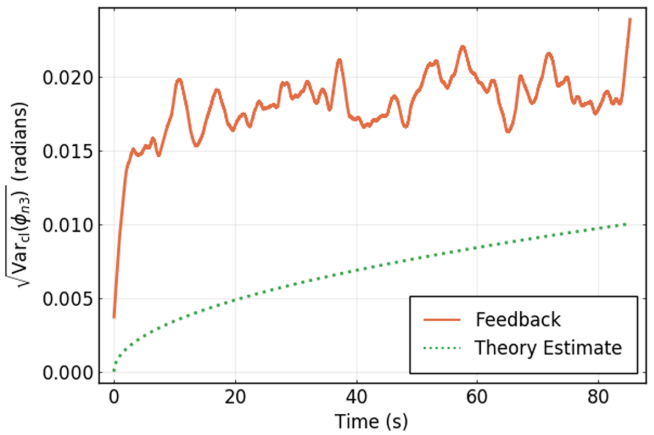

FIG. 5. Phase standard deviation with feedback control applied from the field powered by a Kepco four-quadrant 400 36-12 power supply (solid line). The rms phase deviation rises for a period of less than five seconds, then appears to settle near a fixed value. For comparison, the theoretical estimate (dotted line) is computed assuming 400 pT/$\sqrt{\text{Hz}}$ noise that is high-pass filtered at 500 Hz. Data are smoothed for clarity.

the dressing field that are not due to the current; for example, temperature fluctuations may affect the conductivity of the copper flux return, which would in turn alter the dressing field amplitude even if the current amplitude remains constant.

VI. ROBUST DRESSING

While feedback and cross-cell correlation can be employed to reduce the impact of magnetic field fluctuations which are homogeneous across the measurement cells, these strategies do not mitigate decoherence caused by magnetic field gradients in either the static or dressing field. Thus, we now turn our attention to strategies to amplify coherence times of systems undergoing fluctuating fields, particularly in the presence of magnetic field gradients. The dressing scheme presented in this section is a different technique which, among other applications, can be used to mitigate gradient decoherence of the dressed spins. In this scheme, we apply modulation with angular frequency ω_m to the dressing parameter $x = \gamma B_1/\omega$, where ω_m is faster than the dressed Larmor precession ω_0'. This differs from the modulated CSD presented in Refs. [3,8,9] in that our modulation frequency is much higher. We find that by tuning the rate and amplitude of modulation in conjunction with the dressing parameters B_1 and ω so that there is no phase accumulation in the laboratory frame, we can significantly decrease decoherence, similar to what is found in Refs. [4,5,7]. In a system with two spin species, these parameters can be selected such that both states on a short timescale are rapidly oscillating but on average are effectively frozen in time with respect to the laboratory frame. With this combination of fast oscillation and no phase accumulation in the laboratory frame, quantum states become especially robust to field fluctuations. On average, both spin species remain fixed on the Bloch sphere in the laboratory frame for arbitrary long timescales limited by the coherence. This technique may prove useful in storing quantum information by keeping the state static and robust to electromagnetic fluctuations.

For the nEDM@SNS experiment, the extended coherence time afforded by robust dressing is a valuable tool to rapidly identify and compensate for large magnetic field gradients. The nEDM@SNS experiment is performed in a large cryogenic apparatus; as such, modifications to the apparatus require a long dead time to allow the apparatus to warm, and then cool to its operating temperature ($T < 500$ mK). Thus, it is crucial to be able to mitigate gradients in the measurement cell without the need to make modifications to the apparatus. Aside from robust dressing, nEDM@SNS has two techniques available to measure static magnetic field gradients. First, for stray static field gradients in the precession volume, gradients can be determined by the cryogenic probe array described in Ref. [13]. This array consists of 39 fluxgate magnetometers which will reconstruct the magnetic field by fitting the coefficients of a harmonic scalar potential expansion to the magnetic field values measured by the probes. However, if the ideal static uniform field is distorted by magnetic materials within the volume of interest, the described probe array will not be sufficient to reconstruct the field due to the reconstruction condition that there be no magnetic sources within the volume of interest. Second, gradients can be determined by measuring transverse relaxation rates versus the applied field. However, during the initial phases of the experiment, there may be static field gradients large enough that the scintillation signal decays too quickly to be measured effectively. Such gradients may be caused, for example, by an unknown nickel flash (nickel coating) on an electric connection close to the measurement cell. In the following sections, we first outline a form of precession-free dressing, which we call robust dressing because it is particularly robust against relaxation and dressing field noise. This is due to the fact that a spin undergoing robust dressing does not accumulate phase in the laboratory frame and remains fixed on the Bloch sphere. The longer relaxation time of the robustly dressed system allows us to measure larger gradients than would normally be possible. These results are similar to those obtained for multiple field dressing in Refs. [6,7]. While these references consider dressing fields acting along multiple axes, here we limit ourselves to a single dressing field in the $\hat{x}$ direction, as is the case for the nEDM@SNS experiment. We apply this technique to find precession-free dressing for both ^{3}He and neutron simultaneously, which we call robust critical dressing (RCD).

A. Description within the Bessel function approximation

The dressed system of a single species can be held at a value where no phase accumulates in the laboratory frame, around the zero crossing of the Bessel function, $J_0(\gamma B_1/\omega) \approx 0$. This is described in detail in Ref. [14] for a number of multiple spin systems to achieve a Zeeman-insensitive optical clock atomic transition. Alternatively, the dressing parameter can be modulated between values that achieve a system where no phase accumulation occurs in the laboratory frame. For example, the effective absolute phase of the neutron is approximately

$$\phi_n(t) = \int_0^t \gamma_n J_0\left(\frac{\gamma_n B_1(t)}{\omega}\right) B_0 dt. \tag{85}$$

There are many possible choices for $B_1(t)$. Here we choose $B_1(t)$ to be a constant plus a cosine of frequency ω_m, so that

$$\phi_n(t) = \int_0^t \gamma_n J_0 \left\{ \frac{\gamma_n B_1}{\omega} \left[x_0 + \frac{x_1}{2}(1 + \cos \omega_m t) \right] \right\} B_0 dt, \quad (86)$$

for dimensionless parameters x_0 and x_1. Robust dressing is achieved when there is no phase accumulation in the laboratory frame,

$$\langle \phi_n(t) \rangle = 0, \quad (87)$$

parameters for which can be found numerically. The parameters required to achieve robust dressing in simulations with cosine modulation can be estimated from Eqs. (86) and (87) by integration of the modulation function over a modulation period; moderate deviations from the values predicted analytically are expected due to violation of the Landau-Zener approximation. This is described in the context of spin dressing in Ref. [15]. It is found that the shorter the modulation period, the further the RCD parameters deviate from the analytic prediction. In the simple analytic formulation, it is found that if $x_0 = 1.2$ and $x_1 \approx 3.17$, then $\langle \phi_n(t) \rangle \approx 0$ (for both the neutron and ^{3}He). Despite violation of the Landau-Zener approximation, detailed simulations of the Bloch equation find a continuum of values for x_0 and x_1 that satisfy the robust dressing condition, $\langle \phi_n(t) \rangle = 0$. Deviations away from the average phase can be made small when $\omega_0' < \omega_m$. The average projection of the spin on the Bloch sphere remains fixed, with fluctuations on the order of the modulation period and the instantaneous precession rate.

1. Robustness

Robust dressing suppresses transverse relaxation due to field fluctuations in B_z and B_y. For B_z, this can be seen from the dressing approximation—the effective gyromagnetic ratio under precession-free dressing is zero, and therefore the local static field strength is irrelevant. Likewise, a variation in B_y can be viewed as a rotation of the static field, which in the case where the effective gyromagnetic ratio is zero has no effect on the spins' overall behavior. Thus, the only static gradients and field offsets which contribute to the transverse relaxation rate are those in B_x along any direction. To analyze these, it is useful to consider a simplified model of robust dressing.

B. An intuitive model of robust dressing

While we are not aware of any purely analytical solutions for the robust dressing field, robust dressing has several properties that allow for a convenient approximation. We have chosen the modulation frequency ω_m such that it evenly divides the dressing field frequency ω. Thus, the pulse is periodic with frequency ω_m, and its behavior is entirely defined by its action on a spin during the interval $t = 0$ to $t = 2\pi/\omega_m$. This property allows us to analyze this pulse using Floquet theory, described in Ref. [16]. In short, Floquet's theorem allows us to write the time evolution operator of robust dressing as

$$T(t) = M(t) e^{-i\Lambda t}, \quad (88)$$

where $M(t)$ is a unitary operator with period $2\pi/\omega_m$ and Λ is a time-independent Hermitian operator. The operator Λ can then be written in the form

$$\Lambda = -\tfrac{1}{2}\gamma \vec{B}_{\text{eff}} \cdot \vec{\sigma}. \quad (89)$$

The overall rotation under robust dressing can thus be treated as arising due to an effective magnetic field $\vec{B}_{\text{eff}}$. The effective magnetic field $\vec{B}_{\text{eff}}$ can be computed by numerical integration of the Bloch equations over a single period, or approximated perturbatively as in Refs. [6] and [7].

Numerically, we find that robust dressing corresponds to a weak ($|\gamma B_{\text{eff}}| \approx 1$ Hz) magnetic field whose primary component is in the $\hat{x}$ direction. The precise orientation of $\vec{B}_{\text{eff}}$ may be adjusted by careful selection of the robust dressing parameters.

In light of this, we analyze relaxation in the robust dressing scenario by treating $\vec{B}_{\text{eff}}$ as an effective static uniform field which lies along $\hat{x}$ and redefining T_1 and T_2 accordingly. We also define ϕ to be the angle between the spin and $\hat{x}$. A geometrical representation of the robust dressed system for a neutron is shown in Fig. 6.

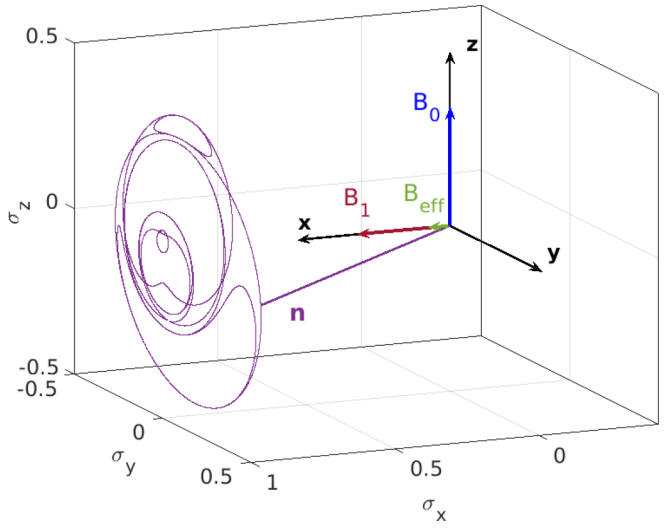

FIG. 6. A classical visualization of the neutron spin trajectory undergoing robust dressing on the Bloch sphere in the laboratory frame, with arrows representing the static uniform field B_0, the dressing field B_1, and the robust dressing effective field B_{eff}.

C. Robust dressing applications

Before presenting an analysis of relaxation under robust dressing, we describe several applications of robust dressing for an nEDM search such as the nEDM@SNS experiment.

1. Gradient metrology through spin relaxation

Because the effects of gradients in B_y and B_z along any direction are suppressed by robust dressing, T_2 is always much shorter than T_1 for the nEDM@SNS experiment's expected operating and initial commissioning conditions. This will lead to a fast initial decay dominated by T_2, followed by a slower decay whose rate is given by T_1. In general, the polarization of spins decays as

$$P(t) = \sqrt{e^{-\frac{2t}{T_1}} \cos^2 \phi_0 + P_{T_2}^2(t) \sin^2 \phi_0}, \quad (90)$$

where $P_{T_2}(t)$ is the component of the polarization transverse to $\hat{x}$ and ϕ_0 is the value of ϕ at the onset of robust dressing. The transition between fast and slow decay then occurs at polarization $P_0 \approx \cos(\phi_0)$. This behavior can be applied for gradient metrology, as a gradient in B_x will cause the spins to relax quickly to a known value, while robust dressing extends the coherence of the system from gradients in B_y or B_z. For the nEDM@SNS experiment, a static magnetic gradient of any field transverse to the static uniform field direction along the dressing axis represents the largest potential systematic effect by generating a frequency shift linear in the applied electric field, as evidenced by Refs. [3,11,17–23]. If this precise gradient measurement technique is used to feedback on magnetic gradient shimming, a powerful mitigation strategy for this linear-in-E frequency shift is achieved.

D. Relaxation under robust dressing

The longitudinal relaxation of the system can be decomposed into two contributions. One contribution arises from the Redfield-like longitudinal decay, which is generated from field imperfections in B_y and B_z, and which we compute by evaluating the system in the interaction picture, similar to the dual harmonic dressing treatment provided by Ref. [7], but with the oscillating field in only the $\hat{x}$ direction. A derivation is found in Appendix F. The model predicts relaxation to be extended beyond the T_1 time found in Refs. [24,25] for the corresponding static uniform field of the nEDM@SNS experiment's operating parameters, discussed in Ref. [9]. This is because the integral over the field correlation function is shifted in frequency according to the harmonics of the dressing field and not the static uniform field as is the case in Ref. [24]. An expansion of the spin's reaction to the applied field into a Fourier series is used to formulate the longitudinal relaxation rate. In the diffusion limit, we find

$$\frac{1}{T_1} \approx \gamma^2\left(G_y^2 + G_z^2\right) D \sum_n \frac{|a_n|^2}{n^2\omega_m^2}, \tag{91}$$

where a_n are the Fourier coefficients of the series and are found numerically. This result can be extended beyond the diffusion limit by using the spectrum of the trajectory autocorrelation function; this is described in Appendix F.

An additional source of longitudinal relaxation arises from the field imperfections in B_x, which generate longitudinal relaxation by rotating the local effective field off of the x direction, resulting in a contribution of the effective field along y and/or z. This in turn will cause relaxation according to

$$\frac{1}{T_1} \approx (G_{\perp,\text{eff}})^2 \frac{D}{|B_{0,\text{eff}}|^2} \tag{92}$$

$$\approx \gamma^2 \left(\frac{\partial B_{\perp,\text{eff}}}{\partial B_x}\right)^2 G_x^2 \frac{D}{|B_{0,\text{eff}}|^2}, \tag{93}$$

where $G_{\perp,\text{eff}}$ and $B_{\perp,\text{eff}}$ refer to components of the effective gradient and magnetic field orthogonal to the effective static uniform field $B_{0,\text{eff}}$. The validity of this estimate depends on the magnitude of gradients in B_x in the cell. In particular, if L_x is the length of the cell along the x direction, then this approximation breaks down when $|G_x L_x/2| \gtrsim |B_{\text{eff}}|$ because the scaling of $B_{\perp,\text{eff}}$ with B_x becomes nonlinear. The longitudinal relaxation will not be proportional to G_x^2, but will scale with a higher power of G_x due to the nonlinearity in the effective field scaling. To find the exact scaling in closed form is difficult. However, it is found from simulations that the robust dressing parameters can be tuned to mitigate this source of relaxation, even for large gradients in B_x. By tuning the robust critical dressing parameters to minimize the relaxation rate, we can mitigate the contribution from the B_x field imperfections to the level of the contribution from the other field directions. With this optimized tuning, the relaxation rate from this gradient returns to G_x^2 scaling, implying a return to the linear scaling of the effective field under optimized robust dressing. Due to the ability to mitigate or increase relaxation by tuning the robust dressing parameters, we find that this modulation technique is a useful form of quantum control.

In practice, because Maxwell's equations require a gradient contribution in at least two directions, this optimization procedure to minimize relaxation obtains diminishing returns when the relaxation from the gradient in B_x becomes comparable in magnitude to the relaxation contributed from gradients in B_y and/or B_z. Due to the nonlinear scaling and the precision of the robust dressing parameters required, we expect that in the large gradient regime, the relaxation from gradients in B_x can be mitigated to parity with the contribution from B_y and B_z. However, in the small gradient regime, where tuning need not be as precise, we may more easily find optimized robust dressing parameters where the contribution from the gradient in B_x can be ignored. The prediction is formulated as

$$\frac{1}{T_1} = C_{dB_x} G_x^2 + \gamma^2\left(G_y^2 + G_z^2\right) D \sum_n \frac{|a_n|^2}{n^2\omega_m^2}, \tag{94}$$

where C_{dB_x} is determined from specifics of the parameters, but, in general, it can be estimated to be of magnitude

$$C_{dB_x} \leqslant \gamma^2 D \sum_n \frac{|a_n|^2}{n^2\omega_m^2}. \tag{95}$$

The relaxation from simulations of a linear gradient, where $G_x = dB_x/dx = -dBz/dz$, is shown in Fig. 7 for all regimes of robust dressing, as well as the theoretical prediction after optimization for both limits of C_{dB_x}. The smallness of B_{eff} compared to B_0 and the nonlinear dependence on G_x lead naturally to three different regimes depending on the magnitude of the G_x gradient relative to B_{eff}.

1. Small gradient regime

If $|G_x L_x/2| \ll |B_{\text{eff}}|$, the magnetic field gradient across the cell is smaller in magnitude than the effective static uniform field. The tuning of the parameters need not be terribly precise ($\delta x_{0,1} \sim x_{0,1} \times 10^{-3}$) to achieve the T_1 relaxation time shown in Eq. (91). Additionally, the G_x contribution to T_1 may be found using the effective magnetic field formalism using Eq. (92).

Similar to traditional nuclear magnetic resonance (NMR) transverse relaxation, the RCD analog can be predicted from Refs. [24,25]; however, only gradients in B_x contribute significantly. Thus, for the transverse polarization, we find

$$P_{T_2}(t) = e^{-\frac{t}{T_2}}, \tag{96}$$

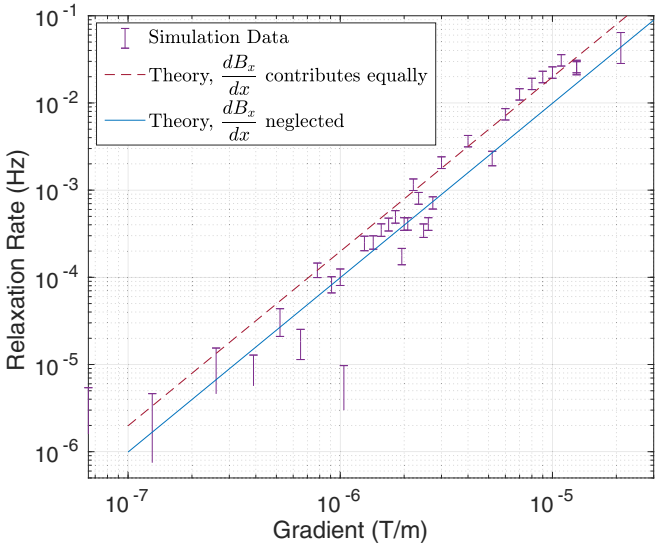

FIG. 7. Relaxation after optimization of robust dressing parameters for 200 Hz robust dressing and a wide range of gradient magnitudes. The gradients in this simulation arise from the divergence theorem, $\frac{dB_z}{dz} = -\frac{dB_x}{dx}$.

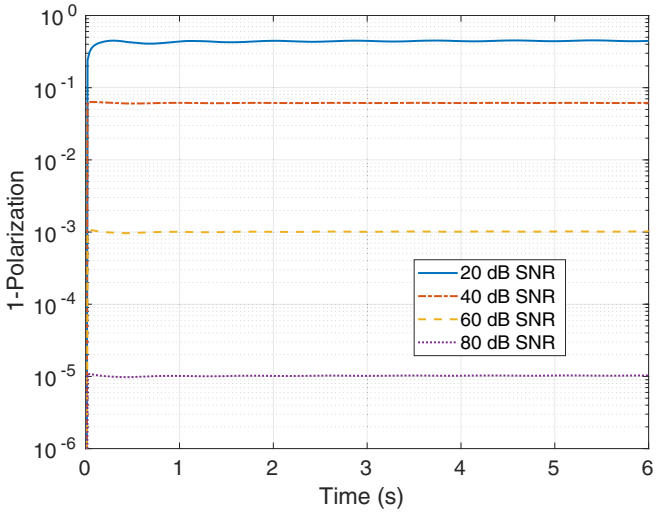

FIG. 8. 1-Polarization for robust dressing modulated according to Eq. (86), where $B_1 = 40.2497\,\mu$T and $\omega_m = 200$ Hz, with simulated noise power varied from 20 to 80 dB SNR.

where, in the diffusion limit,

$$\frac{1}{T_2} = \gamma^2 G_x^2 \frac{L_x^4}{120D}. \tag{97}$$

Outside the diffusion limit, the transverse relaxation can be found from the spectrum of the trajectory autocorrelation function at zero frequency.

2. *Intermediate gradient regime*

If $|G_x L_x/2| \sim |B_{\text{eff}}|$, then the gradient magnetic field nearly cancels B_{eff} in a significant portion of the cell. For untuned robust dressing parameters, the effective magnetic field may have a nonzero $B_{z,\text{eff}}$ component in this region, leading the local magnetic field here to be misaligned with the x axis. This drastically increases the longitudinal relaxation rate for this gradient regime. While no theoretical prediction exists for the dynamics of the spins in this regime, a thorough investigation is presented in Ref. [26]. The strong dependence of T_1 on G_x in the vicinity of the intermediate gradient regime can be employed for gradient metrology. Specifically, a gradient large enough to induce this regime could be identified by measuring the T_1 relaxation of the spin species under study. Although the gradients in B_x required to achieve this regime are a couple of orders of magnitude larger than the initial gradients expected at the onset of commissioning of the nEDM@SNS experiment, they are in the realm of possibility if there is an unaccounted for magnetized material—for example, a nickel flash (nickel coating) on an electrical connection, or other unknown magnetic material close to the measurement cell. Note that while precise ($\delta x_{0,1} \sim x_{0,1} \times 10^{-5}$) tuning of the robust dressing parameters can eliminate the $B_{z,\text{eff}}$ component in the misaligned region, thus recovering the T_1 of Eq. (91), this is not required nor useful for gradient metrology.

3. *Large gradient regime*

As $|G_x L_x/2|$ becomes large compared to $|B_{\text{eff}}|$, the region of low magnetic field shrinks in volume and the effect of misalignment becomes less significant. The treatment of T_1 and T_2 is straightforward. Longitudinal relaxation can be computed from Eq. (91). Transverse relaxation under gradients of this magnitude behave according to the adiabatic regime described in Ref. [27], as the spins dephase on a shorter timescale than the diffusion time. This results in a relatively fast relaxation, given by

$$P_{T_2}(t) = \frac{2}{\gamma G_x L_x t} \sin(\gamma G_x L_x t/2) \tag{98}$$

$$= \text{sinc}\left(\frac{\gamma G_x L_x t}{2}\right), \tag{99}$$

where $\text{sinc}(x) = \frac{\sin(x)}{x}$.

4. *Robust dressing and dressing field noise*

From the simple model that describes robust dressing, we expect that robust dressing is also robust to fluctuations of the dressing field because the integral of the total phase accumulated on average is zero. In simulations of noise, we find that after an initial relaxation period on the timescale of the modulation frequency, the random phase accumulation nearly ceases and dressing field fluctuations arising from power supply noise can typically be ignored with commercial linear amplifiers. The polarization of a robust dressing wave form generated according to Eq. (86), where $B_1 = 40.2497\,\mu$T and $\omega_m = 2\pi \times 200$ rad/s with amplitude noise ranging from 20 to 80 dB SNR, is shown in Fig. 8. In that figure, it is shown that at 20 dB SNR, where the amplitude of the field noise is 10% of the amplitude of the pulse, polarization can be observed for a long time and the rate in Eq. (91) is still achievable after an initial loss.

TABLE II. Optimized parameters for robust critical dressing. All values are calculated for a static uniform field of 5.2 μT and amplitude modulation of a nominal critical dressing field of 40.2497 μT oscillating at 1000 Hz.

$\omega_m/2\pi$ (Hz)	x_0	x_1	$\sqrt{\langle\Delta\theta_{n3}^2\rangle}$ (rad)
200	1.0470	3.1224	0.68
300	1.1005	3.6645	0.41
500	1.3290	3.4435	0.25

5. Robust critical dressing

There exists a nontrivial solution that satisfies the robust dressing conditions for both the neutron and ^{3}He at the same time. Robust critical dressing is achieved when

$$\langle\phi_n\rangle \approx \langle\phi_3\rangle \approx 0. \tag{100}$$

Table II shows optimized robust dressing parameters for the CODATA values of the magnetic moments of the neutron and ^{3}He. We find that robust critical dressing significantly reduces relaxation from field fluctuations in the static uniform field and dressing fields.

Figure 9 shows a simulation of the robust critical dressing signal for $\omega_m = 2\pi \times 200$ Hz in a large gradient, along with the theoretical estimation for robust critical dressing based on

$$\langle\sigma_n \cdot \sigma_3\rangle \approx P_0^2 \exp\left(\gamma_3^2 G_z^2 D t \sum_n \frac{|a_n|^2}{n\omega_m}\right). \tag{101}$$

We have ignored neutron relaxation in this prediction, as it is expected to be small because neutrons exhibit strong motional narrowing. The applied gradient satisfies Maxwell's equations with $dB_z/dz = -dB_x/dx = 2 \times 10^{-2}$ B$_0$/cm. For comparison, unmodulated critical dressing is also simulated

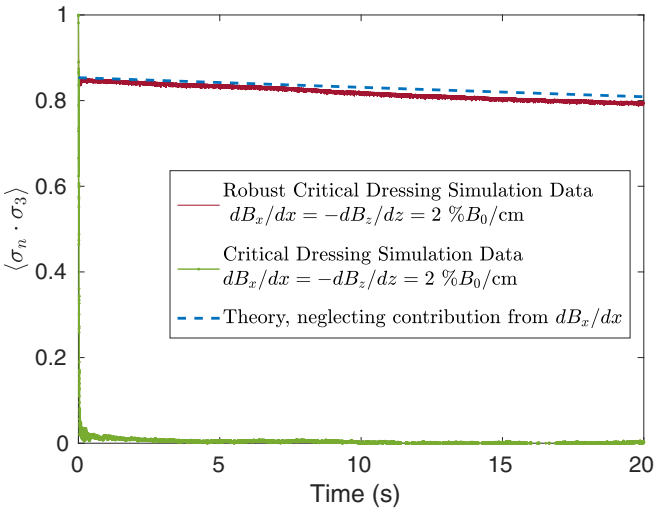

FIG. 9. Simulated signal for highly tuned RCD modulated at 200 Hz (red) and CSD (green), with theoretical estimation for RCD (blue). The starting phase for ^{3}He is $\phi_3 = \pi/8$, and it is the same for neutrons, $\phi_n = \pi/8$. Signal is observable for a long time in the RCD scenario, while the signal is indistinguishable from noise in a traditional critical dressing scenario.

in the same gradient and the signal is found to decay rapidly compared to the robust case.

6. Mitigation of linear-in-E effects

Perhaps the most troublesome systematic effects of EDM experiments is the linear-in-E frequency shift. The linear-in-E frequency shift arises from correlated fluctuations due to the motion of the spin in magnetic field gradients perpendicular to the applied static field, coupled with the $v \times E$ motional magnetic field arising from the motion of the spin within the measurement cell. The effect can be described from second-order perturbation theory in terms of the spectrum of the spin's position-velocity correlation function. An abundance of details concerning this shift is presented in Refs. [3,11,17–23].

Nominally for nEDM@SNS, the electric field is applied parallel to the static uniform field. In this case, robust dressing cannot be used to detect an nEDM. However, if the electric field is instead applied along $\hat{x}$, robust critical dressing can be employed to measure an nEDM and simultaneously mitigate linear-in-E frequency shifts arising from the $v \times E$ motional magnetic field via the same mechanism that mitigates the longitudinal relaxation; specifically, the response of the spin precession system to magnetic field fluctuations is determined by the power spectrum of the noise evaluated at integer multiples of the modulation frequency rather than at the Larmor frequency. Due to the $1/\omega^2$ dependence of the trajectory correlation functions in this regime, described in Ref. [11], the contribution to the linear-in-E frequency shift is significantly mitigated.

VII. CONCLUSION

In this work, we developed a model to evaluate the effect of magnetic field noise on a critically dressed system of neutrons and ^{3}He atoms in the case where the Larmor frequency is a non-negligible fraction of the dressing field frequency. Applying this model to the case of magnetic field fluctuations parallel to the dressing field, we find that the relaxation time is given by an infinite sum over the noise power spectrum evaluated at discrete frequencies, with higher-frequency terms suppressed by higher-order Bessel functions. For the purpose of calculating the impact of current fluctuations in the dressing field coil, these results demonstrate that the primary concern is amplitude fluctuations in the dressing field. These results were verified by numerical integration of the Bloch equations.

With these results as motivation, we propose several strategies to increase coherence and sensitivity for systems of dressed spins. Feedback control of the dressing amplitude, for example, can substantially reduce the phase uncertainty in the presence of current fluctuations in the dressing field coil, while correlating the signal rate from opposing cells allows for rejection of noise sources which are common to both cells. We emphasize that while these strategies are proposed in the context of the nEDM@SNS experiment, these techniques are generally applicable to systems where precise control of dressed spins is required. Of particular interest is robust dressing, which sets the effective Larmor frequency of each species to zero by modulating the dressing field. This substantially reduces relaxation due to magnetic field fluctuations and effectively freezes a state in time which is

useful for extending the coherence of quantum information. Measuring the relaxation of a robustly dressed system allows for precise determination and feedback on gradients parallel to the dressing field, and thus can be applied as gradient metrology for fundamental physics measurements which require a uniform magnetic field. For the nEDM@SNS experiment, this effect can be leveraged to measure or shim relatively large spatial gradients in a critically dressed system of neutrons and ^{3}He. Furthermore, robust dressing allows for mitigation of linear-in-E frequency shifts in EDM experiments where the electric field is chosen to be parallel to the dressing field.

ACKNOWLEDGMENTS

The authors would like to thank Robert Golub, Bradley Filippone, and the nEDM@SNS publications committee for their helpful input and review of the paper. This work was funded by the National Science Foundation Grants No. 1812340 and No. 2110898.

APPENDIX A: NEAR-FREQUENCY TERMS

Suppose $V_I(t)$ contains a pair of terms with frequencies ω_j and ω_k which are very close in frequency, such that $|\omega_j - \omega_k| \sim 1/t$. Then the cross-frequency term can no longer be neglected. Define the integral

$$v_{jk} \equiv \int_0^t dt' \int_0^{t'} dt'' e^{-i\omega_j t'} e^{i\omega_k t''} \langle \delta B(t') \delta B(t'') \rangle. \tag{A1}$$

Using Eq. (9), v_{jk} can be written in terms of the noise power spectrum as

$$v_{jk} = \frac{e^{-2i\Delta\omega t} - 1}{-2i\Delta\omega} \left[\frac{1}{2} S(\bar{\omega}) - \frac{i}{2\pi} \int_{-\infty}^{\infty} d\omega' \frac{S(\omega')}{\omega' - \bar{\omega}} \right].$$

Then the cross terms of $T^\dagger A T$ are

$$\begin{aligned}
&\int_0^t \int_0^t dt' dt'' (Q_j e^{-i\omega_j t''} + Q_j^\dagger e^{i\omega_j t''}) A (Q_k e^{-i\omega_k t'} + Q_k^\dagger e^{i\omega_k t'}) - \int_0^t dt' \int_0^{t'} dt'' (Q_j e^{-i\omega_j t''} + Q_j^\dagger e^{i\omega_j t''})(Q_k e^{-i\omega_k t'} + Q_k^\dagger e^{i\omega_k t'}) A \\
&\quad - \int_0^t dt' \int_0^{t'} dt'' A (Q_k e^{-i\omega_k t'} + Q_k^\dagger e^{i\omega_k t'})(Q_j e^{-i\omega_j t''} + Q_j^\dagger e^{i\omega_j t''}) + (j \leftrightarrow k) \\
&= Q_j A Q_k^\dagger (v_{jk} + v_{kj}^*) + Q_j^\dagger A Q_k (v_{kj} + v_{jk}^*) - Q_j Q_k^\dagger A v_{kj}^* - Q_j^\dagger Q_k A v_{kj} - A Q_k Q_j^\dagger v_{kj} - A Q_k^\dagger Q_j v_{kj}^* + (j \leftrightarrow k) \\
&= v_{jk} (Q_j A Q_k^\dagger + Q_k^\dagger A Q_j - Q_k^\dagger Q_j A - A Q_j Q_k^\dagger) + v_{jk}^* (Q_k A Q_j^\dagger + Q_j^\dagger A Q_k - Q_k Q_j^\dagger A - A Q_j^\dagger Q_k) + (j \leftrightarrow k) \\
&= v_{jk} [Q_k^\dagger, [A, Q_j]] + v_{jk}^* [Q_k, [A, Q_j^\dagger]] + (j \leftrightarrow k).
\end{aligned}$$

1. Explicit calculation for case of static gradients

We first consider noise near the dressed Larmor frequency ω_0'. Using $Q_j = \frac{\gamma}{2}\sigma_{+,1}$ and $Q_k = \frac{\gamma}{2}\sigma_{+,2}$, we get

$$\begin{aligned}
\langle \vec{\sigma}_1 \cdot \vec{\sigma}_2 \rangle &= 1 - \frac{\gamma^2}{4}(v_1 + v_1^* + v_2 + v_2^*) \\
&\quad - \frac{\gamma^2}{4}(v_{kj}^* + v_{kj} + v_{jk} + v_{jk}^*) \\
&= 1 - \frac{\gamma^2}{2} t S(\bar{\omega}) - \frac{\gamma^2}{4} \frac{\sin(2\Delta\omega t)}{\Delta\omega} S(\bar{\omega}) \\
&= 1 - \frac{\gamma^2}{2} S(\bar{\omega}) \left(t - \frac{\sin(2\Delta\omega t)}{2\Delta\omega} \right).
\end{aligned}$$

Next, we consider the contribution of noise near ω, the dressing field frequency. In this case, static gradients do not affect the time dependence of the noise Hamiltonian—that is, the frequency of the complex exponential $e^{i\omega t}$ is unaffected by a change in ω_0 or B_1 (see Sec. III C). Therefore, there are no cross-frequency terms to consider and so noise near ω which applies equally to both cells cannot cause the spins between the two cells to decorrelate.

APPENDIX B: TRANSFORMATION OF THE SIGNAL RATE INTO THE INTERACTION PICTURE

Computing the variance of $\sigma_1 \cdot \sigma_2$ in the laboratory frame corresponds to computing the variance of $U_1 U_2 e^{iHt} \sigma_1 \cdot \sigma_2 e^{-iHt} U_2^\dagger U_1^\dagger$ in the interaction picture. We begin by calculating $U_1 U_2 \sigma_1 \cdot \sigma_2 U_2^\dagger U_1^\dagger$.

From the definition of U_1,

$$\begin{aligned}
U_1 &= D(\eta_1/2) |+_x\rangle \langle +_x| + D^\dagger(\eta_1/2) |-_x\rangle \langle -_x| && \text{(B1)} \\
&= \tfrac{1}{2} D(\eta_1/2)(1 + \sigma_x) + \tfrac{1}{2} D^\dagger(\eta_1/2)(1 - \sigma_x). && \text{(B2)}
\end{aligned}$$

The Pauli spin operators then transform as

$$U_1 \sigma_x U_1^\dagger = \sigma_x, \tag{B3}$$

$$U_1 \sigma_y U_1^\dagger = \tfrac{1}{2}[D(\eta_1) + D^\dagger(\eta_1)]\sigma_y + \tfrac{1}{2} i [D(\eta_1) - D^\dagger(\eta_1)]\sigma_z, \tag{B4}$$

$$U_1 \sigma_z U_1^\dagger = \tfrac{1}{2}[D(\eta_1) + D^\dagger(\eta_1)]\sigma_z - \tfrac{1}{2} i [D(\eta_1) - D^\dagger(\eta_1)]\sigma_y. \tag{B5}$$

So the observable $\sigma_1 \cdot \sigma_2$ transforms as

$$\begin{aligned}
&U_1 U_2 (\sigma_1 \cdot \sigma_2) U_2^\dagger U_1^\dagger \\
&\quad = (U_1 \sigma_{x1} U_1^\dagger)(U_2 \sigma_{x2} U_2^\dagger) + (U_1 \sigma_{y1} U_1^\dagger)(U_2 \sigma_{y2} U_2^\dagger) \\
&\qquad + (U_1 \sigma_{z1} U_1^\dagger)(U_2 \sigma_{z2} U_2^\dagger) && \text{(B6)} \\
&\quad = \sigma_{x1}\sigma_{x2} && \text{(B7)} \\
&\qquad + \frac{1}{2}[D(\Delta\eta) + D^\dagger(\Delta\eta)](\sigma_{y1}\sigma_{y2} + \sigma_{z1}\sigma_{z2}) && \text{(B8)} \\
&\qquad - \frac{i}{2}[D(\Delta\eta) - D^\dagger(\Delta\eta)](\sigma_{y1}\sigma_{z2} - \sigma_{z1}\sigma_{y2}), && \text{(B9)}
\end{aligned}$$

where $\Delta\eta = \eta_1 - \eta_2$.

Applying the approximation in Eq. (51), we have that

$$D(\Delta\eta) \approx \sum_{n,q} J_q(x_1 - x_2)\,|n+q\rangle\,\langle n|\,. \tag{B10}$$

For the fiducial nEDM@SNS experimental parameters, the dressing parameters of the neutrons and ^{3}He atoms are, respectively,

$$x_n \approx -1.184, \quad x_3 \approx -1.317.$$

Because $|x_n - x_3|$ is significantly smaller than 1, the magnitude of $J_q(x_n - x_3)$ is small for $|q| > 0$. For example,

$$J_0(x_n - x_3) = 0.9956, \quad J_1(x_n - x_3) = 0.0662,$$
$$J_2(x_n - x_3) = 0.0022.$$

We therefore make the approximation that

$$U_1 U_2 (\sigma_1 \cdot \sigma_2) U_2^\dagger U_1^\dagger \approx \sigma_1 \cdot \sigma_2. \tag{B11}$$

Next, we need to compute $e^{iH_U t}\sigma_1 \cdot \sigma_2 e^{-iH_U t}$, where we define $H_U = U_2 U_1 H U_1^\dagger U_2^\dagger$. We make use of the identity

$$\begin{aligned} &e^{iH_U t}\sigma_1 \cdot \sigma_2 e^{-iH_U t} \\ &\quad = \sum_{n,n',s_1,s_1',s_2,s_2'} \widetilde{|n, s_1, s_2\rangle}\widetilde{\langle n', s_1', s_2'|}\widetilde{\langle n_1, s_1, s_2|}\sigma_1 \\ &\qquad \cdot \sigma_2 \widetilde{|n', s_1', s_2'\rangle} e^{i\Delta\omega t}, \end{aligned} \tag{B12}$$

where, as before, $\Delta\omega$ is the frequency difference between the states $\widetilde{|n, s_1, s_2\rangle}$ and $\widetilde{|n', s_1', s_2'\rangle}$. We make two simplifications to this expression. First, we are concerned with the time-averaged signal and therefore we ignore any terms where $\Delta\omega \neq 0$. Second, we consider only the leading-order terms in ω_0'/ω and therefore make the approximation that $\widetilde{|n, s_1, s_2\rangle} \approx |n\rangle\,|s_1\rangle\,|s_2\rangle$. The expression in (B12) then becomes

$$\begin{aligned} &\left(e^{iH_U t}\sigma_1 \cdot \sigma_2 e^{-iH_U t}\right)_{\Delta\omega=0} \\ &\quad = \sum_{n,n',s_1,s_1',s_2,s_2'} |n\rangle\,|s_1\rangle\,|s_2\rangle\,\langle n'|\,\langle s_1'|\,\langle s_2'|\,\langle n_1|\,\langle s_1|\,\langle s_2|\,\sigma_1 \\ &\qquad \cdot \sigma_2\,|n'\rangle\,|s_1'\rangle\,|s_2'\rangle\,\delta_{n,n'}\delta_{s_1+s_2,s_1'+s_2'}. \end{aligned} \tag{B13}$$

It turns out that $\langle s_1|\,\langle s_2|\,\langle n|\,\sigma_1 \cdot \sigma_2\,|n'\rangle\,|s_1'\rangle\,|s_2'\rangle = 0$ for $n \neq n'$, and for $s_1 + s_2 \neq s_1' + s_2'$. Therefore,

$$\left(U_1 U_2 e^{iHt}\sigma_1 \cdot \sigma_2 e^{-iHt} U_2^\dagger U_1^\dagger\right)_{\Delta\omega=0} = \sigma_1 \cdot \sigma_2. \tag{B14}$$

APPENDIX C: CALCULATION OF VARIANCE

If a random variable X can be written as a Taylor expansion in some small parameter λ, i.e.,

$$X = \sum_{n=1}^{\infty} \lambda^n Y_n, \tag{C1}$$

where Y_n are random variables, then, to second order in λ, the variance of X is simply $\mathrm{Var}(X) = \lambda^2 \mathrm{Var}(Y)$. Therefore, to compute the variance of $T^\dagger A T$, we need only compute the variance of the terms of $T^\dagger A T$ which are linear in $\delta B(t)$. We get

$$\mathrm{Var}_{cl}(T^\dagger A T) = \mathrm{Var}_{cl}\left[i\int_0^t dt' V_I(t')A - A V_I(t')\right] \tag{C2}$$

$$= \mathrm{Var}_{cl}\left[i\int_0^t dt'(Qe^{-i\omega t} + Q^\dagger e^{i\omega t})A - A(Qe^{-i\omega t} + Q^\dagger e^{i\omega t})\right]\delta B(t') \tag{C3}$$

$$= \mathrm{Var}_{cl}[i([Q, A]u + [Q^\dagger, A]u^*)]. \tag{C4}$$

Using the fact that $\langle u\rangle_{\delta B} = 0$, we rewrite this expression as

$$\mathrm{Var}_{cl}(T^\dagger A T) = \langle|\langle([Q, A]u + [Q^\dagger, A]u^*)\rangle|^2\rangle_{\delta B} \tag{C5}$$

$$= \langle(\langle[Q, A]\rangle\langle[A^\dagger, Q^\dagger]\rangle + \langle[Q^\dagger, A]\rangle, \langle[A^\dagger, Q]\rangle)uu^*\rangle_{\delta B} \tag{C6}$$

$$= 2(\langle[Q, A]\rangle\langle[A^\dagger, Q^\dagger]\rangle + \langle[Q^\dagger, A]\rangle, \langle[A^\dagger, Q]\rangle)\mathrm{Re}(v). \tag{C7}$$

If A is Hermitian, then this can be further simplified to

$$\mathrm{Var}_{cl}(T^\dagger A T) = 4\langle[Q^\dagger, A]\rangle\langle[A, Q]\rangle\mathrm{Re}(v). \tag{C8}$$

APPENDIX D: SIGNAL VARIANCE CALCULATION

For $Q_{\omega_0'} = \frac{\gamma_1}{2}\sigma_{-,1} + \frac{\gamma_2}{2}\sigma_{-,2}$, we need to calculate

$$[\vec{\sigma}_1 \cdot \vec{\sigma}_2, \sigma_{-,1}] = \sigma_{z1}\sigma_{x2} - \sigma_{x1}\sigma_{z2} + i(\sigma_{y1}\sigma_{z2} - \sigma_{z1}\sigma_{y2}). \tag{D1}$$

Then,

$$\begin{aligned} &\left[\vec{\sigma}_1 \cdot \vec{\sigma}_2, \frac{\gamma_1}{2}\sigma_{-,1} + \frac{\gamma_2}{2}\sigma_{-,2}\right] \\ &\quad = \frac{1}{2}(\gamma_1 - \gamma_2)[\sigma_{z1}\sigma_{x2} - \sigma_{x1}\sigma_{z2} + i(\sigma_{y1}\sigma_{z2} - \sigma_{z1}\sigma_{y2})]. \end{aligned} \tag{D2}$$

Since $\vec{\sigma}_1 \cdot \vec{\sigma}_2$ is Hermitian, we compute the magnitude squared of the above quantity to find $\mathrm{Var}_{cl}(T^\dagger \vec{\sigma}_1 \cdot \vec{\sigma}_2 T)$:

$$\mathrm{Var}_{cl}(T^\dagger \vec{\sigma}_1 \cdot \vec{\sigma}_2 T)_{\omega_0'}$$

$$= 4\langle[Q_{\omega_0'}^\dagger, A]\rangle\langle[A, Q_{\omega_0'}]\rangle\mathrm{Re}(v) \tag{D3}$$

$$= \tfrac{1}{2}(\gamma_1 - \gamma_2)^2(\langle\sigma_{z1}\sigma_{x2} - \sigma_{x1}\sigma_{z2}\rangle^2 + \langle\sigma_{y1}\sigma_{z2} - \sigma_{z1}\sigma_{y2}\rangle^2)S(\omega_0')t \tag{D4}$$

$$= \tfrac{1}{2}(\gamma_1 - \gamma_2)^2|\hat{z} \times \{\langle\vec{\sigma}_1\rangle \times \langle\vec{\sigma}_2\rangle\}|^2 S(\omega_0')t. \tag{D5}$$

For $Q_\omega = \frac{\gamma_1 J_1(x_1)\omega_1}{2\omega}\sigma_{z1} + \frac{\gamma_2 J_1(x_2)\omega_2}{2\omega}\sigma_{z2}$, we get

$$[\vec{\sigma}_1 \cdot \vec{\sigma}_2, \sigma_{z1}] = 2i(\sigma_{x1}\sigma_{y2} - \sigma_{y1}\sigma_{x2}). \tag{D6}$$

Then,

$$\begin{aligned} &\left(\vec{\sigma}_1 \cdot \vec{\sigma}_2, \frac{\gamma_1 J_1(x_1)\omega_1}{2\omega}\sigma_{z1} + \frac{\gamma_2 J_1(x_2)\omega_2}{2\omega}\sigma_{z2}\right) \\ &\quad = i\left(\frac{\gamma_1 J_1(x_1)\omega_1 - \gamma_2 J_1(x_2)\omega_2}{\omega}\right)(\sigma_{x1}\sigma_{y2} - \sigma_{y1}\sigma_{x2}). \end{aligned} \tag{D7}$$

Thus,

$$\mathrm{Var}_{cl}(T^\dagger \vec{\sigma}_1 \cdot \vec{\sigma}_2 T)_\omega = 4\langle [Q_\omega^\dagger, A]\rangle\langle [A, Q_\omega]\rangle \mathrm{Re}(v) \tag{D8}$$

$$= 2\left(\frac{\gamma_1 J_1(x_1)\omega_1 - \gamma_2 J_1(x_2)\omega_2}{\omega}\right)^2 \times \langle \sigma_{x1}\sigma_{y2} - \sigma_{y1}\sigma_{x2}\rangle^2 S(\omega)t \tag{D9}$$

$$= 2\left(\frac{\gamma_1 J_1(x_1)\omega_1 - \gamma_2 J_1(x_2)\omega_2}{\omega}\right)^2 \times |\hat{z}\cdot\{\langle\vec{\sigma}_1\rangle \times \langle\vec{\sigma}_2\rangle\}|^2 S(\omega)t. \tag{D10}$$

APPENDIX E: INITIAL STATE OF MAGNETIC FIELD

In this analysis, we assume that the magnetic field oscillates sinusoidally with amplitude B_1. However, this leaves some freedom in choosing the phase of magnetic field at time $t = 0$. A magnetic field $B(t) = B_1 \cos(\omega t - \phi)$ corresponds to the coherent state $|\sqrt{\lambda}e^{i\phi}\rangle$, where λ is the average photon number. Because calculations in this work take place in the displaced basis (which is obtained by applying the unitary transformation U to operators in the laboratory frame), we must also apply U to the initial state $|\alpha\rangle|s\rangle$. We first show that for $|\eta| \ll 1$ and $|\alpha| \gg 1$,

$$D(\eta)|\alpha\rangle \approx e^{\eta\alpha^* - \eta^*\alpha}|\alpha\rangle. \tag{E1}$$

We use the identity that for any complex numbers α and η,

$$D(\eta)D(\alpha) = e^{\eta\alpha^* - \eta^*\alpha}D(\alpha)D(\eta). \tag{E2}$$

Therefore,

$$D(\eta)|\alpha\rangle = D(\eta)D(\alpha)|0\rangle \tag{E3}$$

$$= e^{\eta\alpha^* - \eta^*\alpha}D(\alpha)D(\eta)|0\rangle \tag{E4}$$

$$= e^{\eta\alpha^* - \eta^*\alpha}D(\alpha)|\eta\rangle. \tag{E5}$$

Coherent states are given explicitly in terms of the Fock states by

$$|\eta\rangle = e^{-|\eta|^2/2}\sum_{k=0}^{\infty}\frac{\eta^k}{\sqrt{k!}}|k\rangle. \tag{E6}$$

For $\eta \ll 1$, all but the $k = 0$ terms are small, and so we make the approximation $|\eta\rangle \approx |0\rangle$. From this, we conclude that

$$D(\eta)|\alpha\rangle \approx e^{\eta\alpha^* - \eta^*\alpha}D(\alpha)|0\rangle \tag{E7}$$

$$\approx e^{\eta\alpha^* - \eta^*\alpha}|\alpha\rangle. \tag{E8}$$

Now we examine what happens when we apply

$$U = D(\eta)|+_x\rangle\langle+_x| + D(\eta)^\dagger|-_x\rangle\langle-_x|, \tag{E9}$$

where $\eta = \Omega/2\omega$ to the state $|\alpha\rangle|s\rangle$. We get

$$U|\alpha\rangle|s\rangle = D(\eta)|\alpha\rangle|+_x\rangle\langle+_x|s\rangle + D(\eta)^\dagger|\alpha\rangle|-_x\rangle\langle-_x|s\rangle \tag{E10}$$

$$= |\alpha\rangle\left(e^{i\theta}|+_x\rangle\langle+_x|s\rangle + e^{-i\theta}|-_x\rangle\langle-_x|s\rangle\right) \tag{E11}$$

$$= |\alpha\rangle\left(e^{i\theta}|+_x\rangle\langle+_x| + e^{-i\theta}|-_x\rangle\langle-_x|\right)|s\rangle \tag{E12}$$

$$= |\alpha\rangle e^{i\theta\sigma_x}|s\rangle, \tag{E13}$$

where $\theta = \mathrm{Im}(2\eta^*\alpha)$. We thus see that an initial phase ϕ corresponds to a rotation by an angle θ about the x axis.

APPENDIX F: ROBUST DRESSING RELAXATION DUE TO A RELATIVELY STRONG GRADIENT FIELD

The dynamics of the system can be described by

$$\dot{U}_I = e^{i\varphi_x\sigma_x/2}\omega_{\mathbf{0}}\cdot\sigma e^{-i\varphi_x\sigma_x/2}U_I, \tag{F1}$$

where

$$\varphi_x = \gamma_i\int_0^t B_1(t')dt'. \tag{F2}$$

Within this interaction picture, we can write longitudinal relaxation as the decay rate of $\langle\sigma_x\rangle$, which is given by time-dependent perturbation theory as

$$\langle\sigma_x\rangle = 1 - \gamma^2\mathrm{Re}\left\{\int_0^t dt'\int_0^{t'}dt'' e^{-i\varphi_x(t')}e^{i\varphi_x(t'')} \times\langle\delta B(t')\delta B(t'')\rangle\right\}, \tag{F3}$$

where $\delta B(t)$ in this case represents fluctuations in either B_z or B_y. In writing this approximation, we have taken the static uniform field to be small, which allows us to neglect the contribution to T_1 relaxation from B_x. The integral can be evaluated in terms of the Fourier transform of $e^{-i\varphi_x(t)}$, given by

$$e^{-i\varphi_x(t)} = \sum_{n=-\infty}^{\infty}a_n e^{in\omega_m t}, \tag{F4}$$

where ω_m is the modulation frequency. By the same reasoning as in Sec. III A, we need only consider terms that are the same frequency. Thus we get

$$\langle\sigma_x\rangle = 1 - \gamma^2\mathrm{Re}\left\{\int_0^t dt'\int_0^{t'}dt''\sum_n |a_n|^2 e^{in\omega_m(t'-t'')} \times\langle\delta B(t')\delta B(t'')\rangle\right\} \tag{F5}$$

$$= 1 - 2t\sum_n |a_n|^2 S(n\omega_m). \tag{F6}$$

Therefore, we get

$$\frac{1}{T_1} = \frac{\gamma^2}{2}\sum_n |a_n|^2 S(n\omega_m) \tag{F7}$$

$$\approx \gamma^2\left(G_z^2 + G_y^2\right)D\sum_n\frac{|a_n|^2}{(\omega_m n)^2}, \tag{F8}$$

where, in the last step, we took the diffusion approximation to evaluate $S(n\omega_m)$. If the system is not in the diffusion limit, a more exact formulation can be implemented, for example, the spectrum of the correlation function presented in Ref. [11] would allow accurate predictions from the ballistic through the diffusive regimes.

[1] N. Polonsky and C. Cohen-Tannoudji, Quantum interpretation of frequency modulation, J. Phys. France **26**, 409 (1965).

[2] G. Bevilacqua, V. Biancalana, Y. Dancheva, and A. Vigilante, Restoring Narrow Linewidth to a Gradient-Broadened Magnetic Resonance by Inhomogeneous Dressing, Phys. Rev. Appl. **11**, 024049 (2019).

[3] C. M. Swank, E. K. Webb, X. Liu, and B. W. Filippone, Spin-dressed relaxation and frequency shifts from field imperfections, Phys. Rev. A **98**, 053414 (2018).

[4] G. A. Kazakov and T. Schumm, Magic radio-frequency dressing for trapped atomic microwave clocks, Phys. Rev. A **91**, 023404 (2015).

[5] D. W. Booth, J. Isaacs, and M. Saffman, Reducing the sensitivity of Rydberg atoms to dc electric fields using two-frequency ac field dressing, Phys. Rev. A **97**, 012515 (2018).

[6] G. Bevilacqua, V. Biancalana, A. Vigilante, T. Zanon-Willette, and E. Arimondo, Harmonic Fine Tuning and Triaxial Spatial Anisotropy of Dressed Atomic Spins, Phys. Rev. Lett. **125**, 093203 (2020).

[7] G. Bevilacqua, V. Biancalana, T. Zanon-Willette, and E. Arimondo, Harmonic dual dressing of spin-1/2 systems, Phys. Rev. A **105**, 022619 (2022).

[8] R. Golub and S. K. Lamoreaux, Neutron electric-dipole moment, ultracold neutrons and polarized ^{3}He, Phys. Rep. **237**, 1 (1994).

[9] M. Ahmed, R. Alarcon, A. Aleksandrova, S. Baeßler, L. Barron-Palos, L. Bartoszek, D. Beck, M. Behzadipour, I. Berkutov, J. Bessuille, M. Blatnik, M. Broering, L. Broussard, M. Busch, R. Carr, V. Cianciolo, S. Clayton, M. Cooper, C. Crawford, S. Currie, C. Daurer, R. Dipert, K. Dow, D. Dutta, Y. Efremenko, C. Erickson, B. Filippone, N. Fomin, H. Gao, R. Golub, C. Gould, G. Greene, D. Haase, D. Hasell, A. Hawari, M. Hayden, A. Holley, R. Holt, P. Huffman, E. Ihloff, S. Imam, T. Ito, M. Karcz, J. Kelsey, D. Kendellen, Y. Kim, E. Korobkina, W. Korsch, S. Lamoreaux, E. Leggett, K. Leung, A. Lipman, C. Liu, J. Long, S. MacDonald, M. Makela, A. Matlashov, J. Maxwell, M. Mendenhall, H. Meyer, R. Milner, P. Mueller, N. Nouri, C. O'Shaughnessy, C. Osthelder, J. Peng, S. Penttila, N. Phan, B. Plaster, J. Ramsey, T. Rao, R. Redwine, A. Reid, A. Saftah, G. Seidel, I. Silvera, S. Slutsky, E. Smith, W. Snow, W. Sondheim, S. Sosothikul, T. Stanislaus, X. Sun, C. Swank, Z. Tang, R. T. Dinani, E. Tsentalovich, C. Vidal, W. Wei, C. White, S. Williamson, L. Yang, W. Yao, and A. Young, A new cryogenic apparatus to search for the neutron electric dipole moment, J. Instrum. **14**, P11017 (2019).

[10] Athanasios Papoulis, *Probability, Random Variables, and Stochastic Processes* (McGraw Hill, New York, 1965).

[11] C. M. Swank, A. K. Petukhov, and R. Golub, Random walks with thermalizing collisions in bounded regions: Physical applications valid from the ballistic to diffusive regimes, Phys. Rev. A **93**, 062703 (2016).

[12] E. Tiesinga, P. J. Mohr, D. B. Newell, and B. N. Taylor, Fundamental physical constants, https://www.nist.gov/pml/fundamental-physical-constants.

[13] N. Nouri and B. Plaster, Sensitivity requirements for accessing interior magnetic field vector components in neutron electric dipole moment experiments via exterior boundary-value measurements, J. Instrum. **9**, P11009 (2014).

[14] T. Zanon-Willette, E. de Clercq, and E. Arimondo, Magic Radio-Frequency Dressing of Nuclear Spins in High-Accuracy Optical Clocks, Phys. Rev. Lett. **109**, 223003 (2012).

[15] S. Eckel, S. K. Lamoreaux, M. E. Hayden, and T. M. Ito, Time-dependent spin dressing using a ^{3}He atomic beam, Phys. Rev. A **85**, 032124 (2012).

[16] S. R. Barone, M. A. Narcowich, and F. J. Narcowich, Floquet theory and applications, Phys. Rev. A **15**, 1109 (1977).

[17] E. D. Commins, Berry's geometric phase and motional fields, Am. J. Phys. **59**, 1077 (1991).

[18] J. M. Pendlebury, W. Heil, Y. Sobolev, P. G. Harris, J. D. Richardson, R. J. Baskin, D. D. Doyle, P. Geltenbort, K. Green, M. G. D. van der Grinten, P. S. Iaydjiev, S. N. Ivanov, D. J. R. May, and K. F. Smith, Geometric-phase-induced false electric dipole moment signals for particles in traps, Phys. Rev. A **70**, 032102 (2004).

[19] S. K. Lamoreaux and R. Golub, Detailed discussion of a linear electric field frequency shift induced in confined gases by a magnetic field gradient: Implications for neutron electric-dipole-moment experiments, Phys. Rev. A **71**, 032104 (2005).

[20] A. L. Barabanov, R. Golub, and S. K. Lamoreaux, Electric dipole moment searches: Effect of linear electric field frequency shifts induced in confined gases, Phys. Rev. A **74**, 052115 (2006).

[21] S. M. Clayton, Spin relaxation and linear-in-electric-field frequency shift in an arbitrary, time-independent magnetic field, J. Magn. Reson. **211**, 89 (2011).

[22] C. M. Swank, A. K. Petukhov, and R. Golub, Correlation functions for restricted brownian motion from the ballistic through to the diffusive regimes, Phys. Lett. A **376**, 2319 (2012).

[23] A. Guerrero, P. Sanchez-Moreno, and J. S. Dehesa, Electric-dipole-moment-searches: Reexamination of frequency shifts for particles in traps, Phys. Rev. A **84**, 042105 (2011).

[24] A. Redfield, On the theory of relaxation processes, IBM J. Res. Dev. **1**, 19 (1957).

[25] D. D. McGregor, Transverse relaxation of spin-polarized ^{3}He gas due to a magnetic field gradient, Phys. Rev. A **41**, 2631 (1990).

[26] S. D. Stoller, W. Happer, and F. J. Dyson, Transverse spin relaxation in inhomogeneous magnetic fields, Phys. Rev. A **44**, 7459 (1991).

[27] G. Pignol, M. Guigue, A. Petukhov, and R. Golub, Frequency shifts and relaxation rates for spin-1/2 particles moving in electromagnetic fields, Phys. Rev. A **92**, 053407 (2015).